End-to-End Performance Optimization of a Dual-Hop Hybrid VLC/RF IoT System Based on SLIPT

Huijie Peng, Qiang Li, *Member, IEEE*, Ashish Pandharipande, *Senior Member, IEEE*, Xiaohu Ge, *Senior Member, IEEE*, and Jiliang Zhang, *Senior Member, IEEE*

***Abstract*—In order to enhance the service provisioning to users in the indoor environment, a hybrid visible light communication (VLC)/radio-frequency (RF) Internet of Things (IoT) system is proposed based on simultaneous lightwave information and power transfer (SLIPT). A mobile user equipment, which serves as an off-the-grid relay, is able to extract information from the light-emitting diode source and then forward the processed information to the destination far away, thus dividing the signal transmission into two hops. Specifically, the optical signal received at the relay is separated into alternating current and direct current components for information decoding and energy harvesting, respectively, in the first hop. Then, the energy harvested is used to forward the processed source information to the destination by using RF in the second hop. Subject to the constraints imposed on both the average and the peak powers of the source, the end-to-end outage probability of the system is analytically derived in a closed form. On this basis, the minimization of the end-to-end outage probability is formulated as an optimization problem. This problem is then solved with a joint design of the peak amplitude and the direct current bias of the source transmitter, by trading-off between the performance of two successive hops. Simulation results demonstrate that by using the proposed optimal solution, the information flow and energy flow can be dynamically balanced, resulting in significant performance gains in terms of outage probability and throughput.**

***Index Terms*—End-to-end outage probability, hybrid visible light communication (VLC)/radio-frequency (RF) systems, Internet of Things (IoT), performance optimization, simultaneous lightwave information and power transfer (SLIPT).**

Manuscript received January 11, 2021; revised March 4, 2021 and April 12, 2021; accepted May 3, 2021. Date of publication May 14, 2021; date of current version December 7, 2021. This work was supported in part by the Natural Science Foundation of China (NSFC) under Grant 61971461, and in part by the Hubei Provincial Key Research and Development Program under Grant 2020BAA002. This article was presented in part at the IEEE/CIC International Conference on Communications in China (ICCC), Chongqing, China, 2020. *(Corresponding author: Qiang Li.)*

Huijie Peng, Qiang Li, and Xiaohu Ge are with the School of Electronic Information and Communications, Huazhong University of Science and Technology, Wuhan 430074, China (e-mail: m201871864@hust.edu.cn; qli_patrick@hust.edu.cn; xhge@hust.edu.cn).

Ashish Pandharipande is with Signify, 5656 AE Eindhoven, The Netherlands (e-mail: ashish.p@signify.com).

Jiliang Zhang is with the Department of Electronic and Electrical Engineering, The University of Sheffield, Sheffield S1 4ET, U.K. (e-mail: jiliang.zhang@sheffield.ac.uk).

Digital Object Identifier 10.1109/JIOT.2021.3080518

I. Introduction

With the rapid growth of the Internet of Things (IoT), an unprecedented number of devices will become connected [2], [3]. To provide data exchanges among these devices, radio-frequency (RF) technology has been the main connectivity enabler thus far, which has led to a severe strain on the limited usable portion of the RF spectrum [4]–[6]. On the other hand, measurements reveal that 96% of the IoT-based data generation and consumption occurs in indoor environments [7], [8]. This makes visible light communication (VLC) a promising complementary technology to RF, mainly due to the following reasons: 1) VLC is suitable for indoor environment, where illumination and communication can be achieved simultaneously [9], [10]; 2) VLC covers the spectrum from 380 to 780 nm, which is unlicensed and currently underutilized for wireless communications [11], [12]; and 3) VLC is able to provide low-cost high-speed communications with no interference with RF systems, and no health concerns [13], [14]. With these advantages, VLC has been recognized as an attractive option to alleviate the RF spectrum congestion [9]–[15] and to support the sustainable development of IoT [16], [17].

Albeit with the aforementioned advantages, VLC-based IoT systems can operate under diverse application constraints. Above all, the light beam generated by the light-emitting diode (LED) usually covers only a small conical area and the line-of-sight (LOS) transmission could be easily blocked by obstacles [18]–[23]. In order to expand the effective communication coverage of VLC, hybrid VLC/RF approaches have been proposed [18], [19], which have the potential to benefit from the advantages of both techniques. For instance, by deploying an intermediate relay that operates in both modes of VLC and RF, the system reliability as well as the effective communication range can be significantly enhanced [20], [21], which has the potential to be applied, e.g., in indoor/outdoor communication scenarios [22], [23].

Furthermore, given that IoT devices are typically powered by batteries to support mobility, the battery lifetime is a key performance bottleneck of the entire IoT system [24], [25]. However, traditional options to prolong the battery lifetime by using replaceable batteries may not be feasible under many circumstances [26], [27]. As such, an alternative approach has been proposed to scavenge energy from the surrounding environment, e.g., energy harvesting (EH)

from the RF signal radiations [28], [29], from the optical or lightwave signals [30], [31], etc. On this basis, with the lightwave carrying both information and energy, simultaneous lightwave information and power transfer (SLIPT) was first proposed in [32]. This efficient framework is capable of providing illumination, information, and power transfer simultaneously, which has attracted significant research interests recently [30]–[32].

Motivated by the aforementioned studies, in order to alleviate the spectrum scarcity while enhancing the service provisioning to indoor users with constrained energy, we consider a dual-hop hybrid VLC/RF cooperative communication system based on SLIPT in this article. The system under consideration consists of an LED source (S) located indoor and a destination (D) located far away (possibly outdoor). A mobile user equipment, which attempts to extract information from S and then forward the processed information to D, serves as an off-the-grid relay (R) that moves randomly within the coverage of S and operates in both VLC and RF modes.

This system topology can support low to medium rate VLC-based indoor positioning [33]–[35] and light fidelity (Li-Fi) [36]–[38] applications in complex indoor environment, e.g., airport, parking lot, and commercial complex. To be specific, the relay S corresponds to a mobile user equipment, e.g., a trolley, a shopping cart, and a wheel chair, which is able to receive and extract location-based information from the LED source S [33]–[35]. This information is then forwarded to a backstage management system D, which is usually located much further away or probably outdoor [22], [23], through RF transmissions. By gathering and processing the information from different user equipments, smart and customized value-added services can be provided accordingly [13], [14]. For instance, depending on the location and dwell time of the shopping carts in a supermarket, the shopping needs and behaviors of customers can be analyzed, based on which more targeted recommendation can be provided and the placement of goods can be optimized. Additionally, for disabled people on a wheelchair that is able to extract and forward its location, dwell time, or trajectory to the backstage management system, more smart and customized navigation, early warning or first-aid services can be provided reliably and promptly.

The main system features and contributions of our work are summarized as follows.

1) Considering joint utilization of the basic building blocks of cooperative relay, hybrid VLC/RF, and SLIPT, a dual-hop hybrid VLC/RF cooperative communication model is proposed that operates under reasonable assumptions widely adopted in existing works. To be specific, the received optical signal at R is separated into alternating current (ac) and direct current (dc) components, which are used for information decoding (ID) and EH, respectively, in the first hop. A decode-forward (DF) relaying protocol is adopted wherein upon successfully decoding the source information, S uses the energy harvested to forward the decoded source information to D by using RF, in the second hop.
2) Assuming that R is randomly located within the coverage of S, a relay distance threshold for successfully decoding the source information is first defined, based on which the average outage probability of the first-hop VLC transmission from S to R is derived analytically. Then, a best-effort relay transmission scheme is employed and the corresponding outage performance of the second-hop RF transmission from R to D is characterized. Taking into account the distinct channel conditions across the two hops, the random location of R, the decoding status at R, and the energy harvested by R, the end-to-end outage probability of the entire system is obtained in a closed-form expression.
3) Compared to our earlier work in [1], a more challenging optimization problem is formulated in order to minimize the end-to-end outage probability under the constraints imposed by both the average and the peak powers of the LED source. This problem is solved with a joint design of the peak amplitude A and the dc bias B by trading-off the performances of the two successive hops. Simulation results demonstrate that by using the obtained optimal (B^*, A^*), the information flow and the energy flow can be dynamically balanced, thus achieving significant performance gains in terms of outage probability and throughput of the system.

The remainder of this article is organized as follows. The related work is discussed in Section II, where our work is compared with the state of the art. The considered dual-hop hybrid VLC/RF IoT system based on SLIPT is introduced in Section III. In Section IV, the outage performance of the first-hop VLC link and the second-hop RF link are separately analyzed, based on which the end-to-end outage probability of the entire system is obtained in a closed-form expression. In Section V, an optimization problem of minimizing the end-to-end outage probability is first formulated, which is then solved with a sophisticated design of the peak amplitude and the dc bias of the source transmitter. Simulation results are presented in Section VI. Finally, Section VII concludes this article.

II. Related Work

As a promising technique to alleviate the RF spectrum bottleneck, VLC has drawn much research attention recently [9]–[14]. However, before it can be applied to IoT systems, at least two key challenges, imposed by the constrained coverage and energy, need to be addressed.

In order to extend the communication coverage of VLC, a cooperative relay operating in hybrid VLC/RF mode was introduced in [18]–[21] to first receive the VLC signal and then forward it to the intended destination by using RF transmissions. A hybrid VLC/RF system was proposed for wireless access networks in [18], which was shown to be more energy efficient and capable of adapting to the changes in the ambient lighting conditions, as compared to the systems that utilize VLC or RF access methods separately. The dc bias of the VLC transmitter was optimized to maximize the average end-to-end data rate in [19], where a VLC/RF relay is employed with fixed location. Considering the randomness of the locations of the relay and destination, the outage performances of the hybrid VLC/RF systems under amplify-forward (AF)

and DF relaying protocols were, respectively, characterized in [20]. In [21], the statistical characteristics of the received signal-to-noise ratio were characterized, and then, the analytical expressions for exact and asymptotic secrecy outage probability were derived by using a stochastic geometry. In the above studies, different hybrid VLC/RF system models were proposed and the corresponding performance was analyzed from different aspects. However, there lacks a comprehensive analysis on the end-to-end outage performance, where all the relevant factors involved, e.g., the distinct channel conditions across the two hops, the random location of S, the signal processing at S, the energy harvested by S, etc., need to be taken into consideration.

In order to alleviate the bottleneck imposed by the constrained energy, a comprehensive overview on SLIPT-based VLC systems was provided in [39], where different SLIPT receiver architectures were put forward. In [40], the tradeoff between the achievable rate and energy harvested was analyzed for a system with a single transmitter and a single receiver, where dynamic power splitting was used to separate the energy and information streams. In [41], a typical indoor SLIPT-based VLC system, including one transmitter, one desired information receiver, and one energy receiver, was considered, based on which the secrecy outage probability and average secrecy capacity were analyzed, respectively. In [42], a multicell SLIPT system was considered for serving multiple users, where the optimal spectral efficiency-EH tradeoff was investigated. In [43], the illumination rate-energy region was investigated for the point-to-point SLIPT-based VLC systems, based on which the transmission power minimization problem and the minimum rate maximization problem were studied. In the above studies, different tradeoffs were analyzed that reveal the inherent interplays between the information and energy. However, these tradeoffs cannot explicitly reflect the key issues including what are the impacts of the key parameters, and how these key parameters should be configured to improve the end-to-end performance of the system.

In order to support the energy-constrained IoT devices in indoor/outdoor environments, SLIPT has also been investigated in hybrid VLC/RF systems [44]–[46]. In [44], a dual-hop hybrid VLC/RF communication system was considered, where the relay harvested energy in the first-hop VLC link by extracting the dc component from the received signal and then used the energy harvested to empower the transmission to the destination in the second-hop RF link. Pan *et al.* [45] characterized the outage performance of a hybrid VLC/RF system, where the visible light was used for SLIPT in the downlink, and the harvested energy was used to transmit an RF signal in the uplink in return. A hybrid VLC/RF system was considered in [46], where two transmitters communicated with two designated receivers, respectively, through a common relay, which is able to harvest optical energy from the VLC system and perform DF relaying via an RF link to the receivers. Although similar SLIPT-based hybrid VLC/RF models were considered in the aforementioned studies, to the best of our knowledge, our work is the first attempt in the open literature to dynamically balance the information flow and the energy flow over the considered system. By using the obtained optimal approach, the information can be reliably delivered by efficiently utilizing the available energy, thus significantly improving the outage probability and throughput of the system.

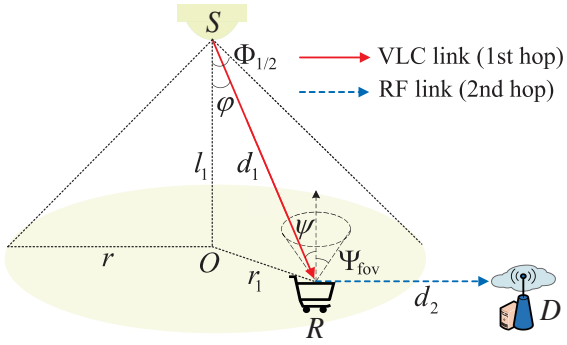

Fig. 1. Illustration of the considered dual-hop hybrid VLC/RF cooperative communication system based on SLIPT, in which an off-the-grid relay R, moving randomly within the coverage of the LED source S, assists in forwarding information to the destination D by using the energy harvested from the lightwave emitted by S.

III. System Model and Protocol Description

The dual-hop hybrid VLC/RF cooperative communication system under consideration is depicted in Fig. 1 and consists of an LED source (S), an off-the-grid relay (R), and a destination (D). Due to the nature of the light beam, the communication coverage area of the LED is assumed as a fixed conical area with a center O and a radius r on the bottom plane where R is located [47]. The relay R, equipped with a photo detector (PD), is assumed to be randomly located on the bottom circle [48]. The destination D is an end user located much further away, and thus, no direct link exists between S and D.

A. First-Hop VLC Signal Transmission

Previous, studies indicate that in a typical indoor environment, the strongest diffuse component is at least 7 dB (electrical) lower than the weakest LOS component [49]. Thus, in order to focus on the end-to-end outage performance analysis and optimization of the considered system, the multipath reflection is ignored and only the LOS link between S and S is considered [47]–[49]. Then, the corresponding channel gain of $S \to R$ can be expressed as [44]–[49]

$$h_1 = \frac{(n+1)}{2\pi d_1^2}(\cos\varphi)^n L_r T_s(\psi) g(\psi) \cos\psi. \tag{1}$$

Here, $n = -\ln 2/(\ln(\cos(\Phi_{1/2})))$ denotes the order of Lambertian emission, where $\Phi_{1/2}$ is the semiangle of the LED. $d_1 = (l_1^2 + r_1^2)^{(1/2)}$ denotes the distance of $S \to R$, where l_1 is the distance of $S \to O$, and r_1 is the distance of $O \to R$. L_r denotes the physical area of the PD, φ denotes the irradiation angle, and ψ denotes the incidence angle. Considering the use case where a shopping cart serves as the mobile relay S, it is reasonable to assume that the transmitter plane is parallel to the receiver one [47]–[49], i.e., $\varphi = \psi = \arctan(r_1/l_1)$. $T_s(\psi)$ denotes the gain of the optical filter, and

$$g(\psi) = \begin{cases} \varepsilon^2/(\sin(\Psi_{fov}))^2, & 0 \le \psi \le \Psi_{fov} \\ 0, & \Psi_{fov} < \psi \end{cases}$$

TABLE I
LIST OF SYMBOLS AND DEFAULT VALUES ADOPTED IN THIS ARTICLE

Symbols	Definitions	Default Values
r	Radius of the circle	3 m [21], [22]
n	Order of Lambertian emission	1 [18]-[20]
$\Phi_{1/2}$	Semi-angle of the LED	60 deg [18]-[20]
l_1, r_1	Distance of $S \to O$, $O \to R$	2 m, $[0, 3]$ m [21], [22]
d_1, d_2	Distance of $S \to R$, $R \to D$	$[2, \sqrt{13}]$ m, 25 m [22]
φ, ψ	Irradiation angle, incident angle	$[0, \arctan\frac{3}{2}]$ deg [49]
L_r	Physical area of the PD	0.6 cm^2 [31], [32]
$T_s(\psi)$	Gain of the optical filter	1 [47]-[49]
$g(\psi)$	Gain of the optical concentrator	4.5 [47]-[49]
ε	Reflective index	1.5 [47]-[49]
Ψ_{fov}	Field of view of the PD	45 deg [47]-[49]
A	Peak amplitude of the signal	5 mA [19], [32]
B	dc bias	10 mA [19], [32]
P_{LED}	LED power	100 mW/A [19], [32]
$P_a, P_{\max}$	Average power, Peak power	3 mW, 4 mW [51]
ξ	Dimming target	$\frac{3}{4}$ [50], [51]
ρ	Photo-detector responsivity	0.6 A/W [52]-[54]
σ_1^2, σ_2^2	Additive white Gaussian noise	10^{-20} W, 10^{-16} W [51]
f	Fill factor	0.75 [19], [21]
V_{oc}	Open circuit voltage of the PD	$V_t \ln\left(1 + \frac{y_{\text{dc}}}{I_0}\right)$ [21]
V_t	Thermal voltage	25 mV [19], [21]
I_0	Dark saturation current of the PD	10^{-9} A [19], [21]
ν	Path-loss exponent	3 [25], [29]
τ	Time slot allocation factor	0.5 [19], [32]
R_t	Pre-defined target rate	1 bit/slot/Hz [31], [49]

denotes the gain of the optical concentrator, where ε is the reflective index and Ψ_{fov} is the Field of View (FoV). For ease of reference, a list of symbols that appear in this article is summarized in Table I, along with their typical values.

Different from traditional communication systems where various modulation schemes can be applied, intensity modulation and direct detection (IM/DD) [9]–[11] are generally employed in VLC systems, where the transmitted waveform is modulated onto the instantaneous power, resulting in a real and positive waveform [12]–[14]. Let $x(t)$ denote the modulated electrical source signal, whose peak amplitude is A. A dc bias B is then added to $x(t)$ to ensure that the resulting signal is nonnegative [9]–[14], before being used to modulate the optical intensity of the LED. The transmitted optical signal can thus be given as

$$x_s(t) = P_{\text{LED}}(x(t) + B) \tag{2}$$

where P_{LED} is the LED power, $x(t) \in [-A, A]$ with the corresponding expectation $\mathbb{E}[x(t)] = 0$, and $(x(t) + B) \geq 0$ [30]–[32]. For safety reasons and practical implementation considerations, two constraints of the average power and peak power have to be met [50], given as

$$\begin{cases} \mathbb{E}[x_s(t)] \leq P_a & \Rightarrow B \leq \frac{P_a}{P_{\text{LED}}} \\ 0 \leq x_s(t) \leq P_{\max} & \Rightarrow A \leq \min\left\{B, \frac{P_{\max}}{P_{\text{LED}}} - B\right\} \end{cases} \tag{3}$$

where P_a and $P_{\max}$ denote the maximum allowed average and peak powers, respectively [51]. In order to describe the illumination requirements in dimmable VLC, we define $\xi \triangleq (P_a/P_{\max})$ as the dimming target. Considering the dimming control that the LED source can arbitrarily adjust light brightness, the dimming target must satisfy $0 < \xi \leq 1$ [50], [51].

B. Signal Processing at the Relay

Based on the above definitions, the output electrical signal $y_r(t)$ of the PD at relay R in the 1st hop can be written as

$$\begin{aligned} y_r(t) &= \rho h_1 x_s(t) + n_1(t) \\ &= \rho h_1 P_{\text{LED}} x(t) + \rho h_1 P_{\text{LED}} B + n_1(t) \\ &= y_{ac}(t) + y_{dc} + n_1(t) \end{aligned} \tag{4}$$

where ρ is the PD responsivity, $y_{ac}(t) = \rho h_1 P_{\text{LED}} x(t)$ is the ac component, and $y_{dc} = \rho h_1 P_{\text{LED}} B$ is the dc component. In addition to the desired LOS signal, R will also receive the ambient light emitted from other sources. The ambient light, after sufficient reflections, refractions and scattering, will reach S via different paths, thus of different angles of arrival, different delays or phases, and different amplitudes [53], [54]. In other words, the noise of the ambient light is the superposition of a large number of statistically independent random variables. Then, according to the central limit theorem, we let $n_1(t)$ denote the noise created from the ambient visible light, background shot noise, and thermal noise, where $n_1(t) \sim \mathcal{CN}(0, \sigma_1^2)$ [50], [51].

Under the signal components separation scheme [39], the received photocurrent at R is split into two streams, with the dc component for EH and the ac component for ID, respectively. The harvested energy is thus expressed as

$$\begin{aligned} E_R &= f y_{dc} V_{oc} \\ &= f \rho h_1 P_{\text{LED}} B V_t \ln\left(1 + \frac{\rho h_1 P_{\text{LED}} B}{I_0}\right) \\ &\approx \frac{f V_t (\rho P_{\text{LED}} B)^2 \gamma_1}{I_0} \qquad (5) \\ &= \frac{f V_t (\rho P_{\text{LED}} B)^2 \left[(n+1) k l_1^{n+1}\right]^2}{I_0 \left(r_1^2 + l_1^2\right)^{n+3}} \qquad (6) \end{aligned}$$

where f is the fill factor whose value is between 0.7 and 0.8 in practice, $V_{oc} = V_t \ln(1 + [y_{dc}/I_0])$ is the open circuit voltage of the PD, $V_t \approx 25$ mV is the thermal voltage, and I_0 is the dark saturation current of the PD. Here, (5) is obtained in that $\ln(1 + [(\rho h_1 P_{\text{LED}} B)/I_0]) \approx [(\rho h_1 P_{\text{LED}} B)/I_0]$, which is an accurate approximation when $[(\rho h_1 P_{\text{LED}} B)/I_0] \to 0$. By letting $\gamma_1 = |h_1|^2$, we have

$$\gamma_1 = \frac{\left[(n+1) k l_1^{n+1}\right]^2}{\left(r_1^2 + l_1^2\right)^{n+3}} \tag{7}$$

where k is a constant given by $k = (1/2\pi) L_r T_s(\psi) g(\psi)$.

On the other hand, S attempts to first retrieve the original signal $x(t)$ from the ac component $y_{ac}(t)$ [32], [49], and then proceeds to forward the decoded source signal $x(t)$ to D by using its energy harvested from the dc component. However, if S fails to decode $x(t)$, then it simply stays silent. Although the energy harvested by S can be possibly kept to the next signal transmission, we omit this case in order to focus on the end-to-end analysis of the outage probability, which will result in a performance lower bound.

C. Second-Hop RF Signal Transmission

We adopt a Rayleigh fading model and let $h_2 \sim \mathcal{CN}(0, d_2^{-\nu})$ denote the channel coefficient in the second hop, where d_2 is the distance between S and D, and ν is the path-loss exponent [25], [29]. Defining d_0 as the distance between the center of the circular area O and D, due to the random location of S, we have $d_2 \in [d_0 - r, d_0 + r]$. In view of the fact that S moves within a very small area compared to its distance to D, for ease of analysis, it is assumed that $d_2 = d_0$ irrespective of the location of S within the circular area. This is a reasonable assumption that ends up with an accurate approximation, especially when $d_0 \gg r$.

Upon successfully decoding the source signal $x(t)$ in the first hop, S proceeds to forward it to D in the second hop. The corresponding received signal at D is given by

$$y_d(t) = \sqrt{P_R} h_2 \frac{x(t)}{\left(A/\sqrt{2}\right)} + n_2(t) \tag{8}$$

where P_R is the transmission power of R, and $n_2(t) \sim \mathcal{CN}(0, \sigma_2^2)$ is the AWGN. Here, $A/\sqrt{2}$ is included in the denominator for the normalization of $x(t)$, where $\mathbb{E}[|x(t)|^2] = A^2/2$.

IV. End-to-End Performance Analysis

Without loss of generality, we assume that the transmissions over $S \to R \to D$ are performed slot-by-slot [18], [19], where each time slot is divided into two phases for $S \to R$ and $R \to D$, respectively, with a factor τ where $0 < \tau < 1$. That is, a fraction τ of a time slot is allocated to the first phase, with the remaining fraction $(1 - \tau)$ of this time slot for the second phase [19], [32]. Then, the corresponding channel capacity of $S \to R$ can be approximated as [50] and [51]

$$C_1 \approx \tau \log_2\left(1 + \frac{\rho^2 (P_{\text{LED}})^2 A^2 \gamma_1}{2\pi e \sigma_1^2}\right). \tag{9}$$

Without knowing the perfect instantaneous channel state information at the transmitter side, the LED source S simply transmits at a predefined target rate R_t [31], [49]. Then, we have the corresponding outage probability of the first hop

$$O_P^{(1)} = \Pr\{C_1 < R_t\}. \tag{10}$$

Upon successfully decoding $x(t)$ in the first hop, the corresponding achievable rate of the second-hop RF transmission from S to D can be expressed from (8) as

$$R_2 = (1 - \tau) \log_2\left(1 + \frac{P_R \gamma_2}{\sigma_2^2}\right) \tag{11}$$

where $\gamma_2 = |h_2|^2$ follows an exponential distribution with probability density function (PDF) $f_{\gamma_2}(\gamma_2) = d_2^{\nu} e^{-d_2^{\nu}\gamma_2}$ and $\gamma_2 > 0$ [25], [29]. Then, we have the corresponding outage probability of the 2nd hop

$$O_P^{(2)} = \Pr\{\{C_1 \geq R_t\} \wedge \{R_2 < R_t\}\}. \tag{12}$$

Next, we analyze the outage performance of the two successive hops, respectively.

A. First-Hop Outage Performance Analysis

1) Relay Distance Threshold $r_{1,th}$: Since S moves randomly within the circular area, the closer S is located to O, i.e., a smaller r_1, the higher capacity C_1 is achieved, and *vice versa*. To characterize the decoding status at S, we define a relay distance threshold $r_{1,\text{th}}$ between O and S. To be specific, if $r_1 \leq r_{1,\text{th}}$, then the source information $x(t)$ can be successfully decoded, i.e., $C_1 \geq R_t$. Otherwise, if $r_1 > r_{1,\text{th}}$, then $C_1 < R_t$.

Based on the above definition, for R to successfully decode $x(t)$ in the first hop, we have from (9)

$$\begin{aligned}
&\tau \log_2\left(1 + \frac{\rho^2 (P_{\text{LED}})^2 A^2 \gamma_1}{2\pi e \sigma_1^2}\right) \geq R_t \\
&\Rightarrow \frac{\left[(n+1) k l_1^{n+1}\right]^2}{\left(r_1^2 + l_1^2\right)^{n+3}} \geq \frac{2\pi e \lambda_1 \sigma_1^2}{\rho^2 (P_{\text{LED}})^2 A^2} \\
&\Rightarrow r_1 \leq r_{1,\text{th}} = \left\{ \left[\frac{\left(\rho P_{\text{LED}} A (n+1) k l_1^{n+1}\right)^2}{2\pi e \lambda_1 \sigma_1^2} \right]^{\frac{1}{n+3}} - l_1^2 \right\}^{\frac{1}{2}}
\end{aligned} \tag{13}$$

where $\lambda_1 = 2^{(R_t/\tau)} - 1$.

2) Average Outage Probability $O_P^{(1)}$: Since S is located randomly and uniformly within the circular area, r_1 follows a PDF $f_{r_1}(r_1) = (2r_1/r^2)$, where $0 \leq r_1 \leq r$ [49]. Then, we have the average outage probability of the first hop

$$\begin{aligned}
O_P^{(1)} &= \Pr\{C_1 < R_t\} \\
&= \Pr\left\{r_{1,\text{th}} < r_1 \leq r\right\} &(14)\\
&= \int_{r_{1,\text{th}}}^{r} f_{r_1}(r_1) dr_1 = 1 - \frac{\left(r_{1,\text{th}}\right)^2}{r^2} &(15)
\end{aligned}$$

where (14) is obtained due to the fact that

$$\Pr\{C_1 < R_t\} = \begin{cases} 0, & 0 \leq r_1 \leq r_{1,\text{th}} \\ 1, & r_{1,\text{th}} < r_1 \leq r. \end{cases} \tag{16}$$

B. Second-Hop Outage Performance Analysis

1) PDF of Harvested Energy E_R at S: Upon successfully decoding $x(t)$ in the first hop, a best-effort transmission scheme is adopted in the second hop [21], [29], i.e., $P_R = E_R$. Next, we analyze the PDF of E_R subject to the random locations of S.

From (7), it is evident that γ_1 is a monotonically decreasing function with respect to r_1, and the inverse function $r_1^{-1}(\gamma_1)$ of γ_1 can be obtained as

$$r_1^{-1}(\gamma_1) = \left\{ \left[\frac{\left((n+1) k l_1^{n+1}\right)^2}{\gamma_1} \right]^{\frac{1}{n+3}} - l_1^2 \right\}^{\frac{1}{2}}.$$

Then, the PDF of γ_1 is [55]

$$f_{\gamma_1}(\gamma_1) = f_{r_1}\left(r_1^{-1}(\gamma_1)\right) \left| \frac{\partial r_1^{-1}(\gamma_1)}{\partial \gamma_1} \right|$$

$$= \frac{2r_1^{-1}(\gamma_1)}{r^2}\left|-\frac{1}{2r_1^{-1}(\gamma_1)}\frac{\left[(n+1)kl_1^{n+1}\right]^{\frac{2}{n+3}}}{n+3}\gamma_1^{\frac{-n-4}{n+3}}\right|$$

$$= \frac{\left[(n+1)kl_1^{n+1}\right]^{\frac{2}{n+3}}}{(n+3)r^2}\gamma_1^{\frac{-n-4}{n+3}}. \tag{17}$$

Then, based on (6), we calculate the PDF of E_R as [55]

$$f_{E_R}(E_R) = f_{\gamma_1}\left(\gamma_1^{-1}(E_R)\right)\left|\frac{\partial\gamma_1^{-1}(E_R)}{\partial E_R}\right|$$
$$= \frac{\left[(n+1)kl_1^{n+1}\right]^{\frac{2}{n+3}}}{(n+3)r^2}\left[\frac{I_0E_R}{fV_t(\rho P_{\mathrm{LED}}B)^2}\right]^{\frac{-n-4}{n+3}} \times\left|\frac{I_0}{fV_t(\rho P_{\mathrm{LED}}B)^2}\right|$$
$$= \alpha E_R^{\frac{-n-4}{n+3}} \tag{18}$$

where $\gamma_1^{-1}(E_R) = [(I_0E_R)/(fV_t(\rho P_{\mathrm{LED}}B)^2)]$ and $\alpha = [(\{fV_t(\rho P_{\mathrm{LED}}B)^2[(n+1)kl_1^{n+1}]^2\}^{\frac{1}{n+3}})/(I_0^{\frac{1}{n+3}}(n+3)r^2)]$.

2) Average Outage Probability $O_P^{(2)}$: From (12) and (14), $O_P^{(2)}$ can be rewritten as

$$O_P^{(2)} = \Pr\left\{\left\{0 \le r_1 \le r_{1,\mathrm{th}}\right\} \wedge \{R_2 < R_t\}\right\}. \tag{19}$$

When $r_1 = 0$ and $r_{1,\mathrm{th}}$, respectively, we have from (6) the corresponding energy harvested by R

$$E_{\max} = \frac{fV_t(\rho P_{\mathrm{LED}}B)^2\left[(n+1)kl_1^{n+1}\right]^2}{I_0l_1^{2(n+3)}} \tag{20a}$$

$$E_{1,\mathrm{th}} = \frac{fV_t(\rho P_{\mathrm{LED}}B)^2\left[(n+1)kl_1^{n+1}\right]^2}{I_0\left[\left(r_{1,\mathrm{th}}\right)^2 + l_1^2\right]^{n+3}}. \tag{20b}$$

Thus, (19) can be further derived as

$$O_P^{(2)} = \int_{E_{1,\mathrm{th}}}^{E_{\max}} f_{E_R}(E_R)\int_0^{\frac{\lambda_2\sigma_2^2}{E_R}} f_{\gamma_2}(\gamma_2)d\gamma_2 dE_R$$
$$= \int_{E_{1,\mathrm{th}}}^{E_{\max}} \alpha E_R^{\frac{-n-4}{n+3}}\left(1 - e^{\frac{-\lambda_2 d_2^v\sigma_2^2}{E_R}}\right)dE_R$$
$$= \int_{E_{1,\mathrm{th}}}^{E_{\max}} \alpha E_R^{\frac{-n-4}{n+3}}dE_R - \int_0^{E_{\max}} \alpha E_R^{\frac{-n-4}{n+3}}e^{\frac{-\beta}{E_R}}dE_R + \int_0^{E_{1,\mathrm{th}}} \alpha E_R^{\frac{-n-4}{n+3}}e^{\frac{-\beta}{E_R}}dE_R \tag{21}$$
$$= \frac{\left(r_{1,\mathrm{th}}\right)^2}{r^2} - \alpha\beta^{\frac{-n-4}{2(n+3)}}(E_{\max})^{\frac{n+2}{2(n+3)}}e^{\frac{-\beta}{2E_{\max}}}\mathcal{W}_{\frac{-n-2}{2(n+3)},\frac{-1}{2(n+3)}}\left(\frac{-\beta}{E_{\max}}\right) + \alpha\beta^{\frac{-n-4}{2(n+3)}}\left(E_{1,\mathrm{th}}\right)^{\frac{n+2}{2(n+3)}}e^{\frac{-\beta}{2E_{1,\mathrm{th}}}}\mathcal{W}_{\frac{n-2}{2(n+3)},\frac{-1}{2(n+3)}}\left(\frac{-\beta}{E_{1,\mathrm{th}}}\right) \tag{22}$$

where $\lambda_2 = 2^{(R_t/(1-\tau))} - 1$, $\beta = \lambda_2 d_2^v\sigma_2^2$, and $\mathcal{W}_{u,(1/2)+u}(z) = z^{-u}e^{(1/2)z}\int_z^\infty t^{2u}e^{-t}dt$ is the Whittaker function [56, eq. (9.224)].

C. End-to-End Outage Probability

From (10) and (12), since $\{C_1 < R_t\}$ and $\{\{C_1 \ge R_t\}\wedge\{R_2 < R_t\}\}$ are mutually exclusive, the end-to-end system outage probability can be obtained with a summation of $O_P^{(1)}$ and $O_P^{(2)}$ obtained in (15) and (22), respectively, given as

$$O_P = 1 - \alpha\beta^{\frac{-n-4}{2(n+3)}}(E_{\max})^{\frac{n+2}{2(n+3)}}e^{\frac{-\beta}{2E_{\max}}}\mathcal{W}_{\frac{-n-2}{2(n+3)},\frac{-1}{2(n+3)}}\left(\frac{-\beta}{E_{\max}}\right) + \alpha\beta^{\frac{-n-4}{2(n+3)}}\left(E_{1,\mathrm{th}}\right)^{\frac{n+2}{2(n+3)}}e^{\frac{-\beta}{2E_{1,\mathrm{th}}}}\mathcal{W}_{\frac{-n-2}{2(n+3)},\frac{-1}{2(n+3)}}\left(\frac{-\beta}{E_{1,\mathrm{th}}}\right). \tag{23}$$

D. Average Throughput and Energy Efficiency

From (23), the average throughput achieved by the proposed system, which is defined as the amount of successfully delivered data bits per time slot [57], [58], can be obtained as

$$T_P = (1 - O_P)R_t. \tag{24}$$

On this basis, the energy efficiency achieved by the proposed system, which is defined as the ratio between the amount of data bits successfully delivered and the transmission energy consumed by the LED source [59], [60], can be obtained as

$$\eta_E = \frac{T_P}{\tau\mathbb{E}[x_s(t)]} = \frac{(1 - O_P)R_t}{\tau P_{\mathrm{LED}}B}. \tag{25}$$

V. Optimization of the End-to-End Outage Performance

A. Problem Formulation

1) Effects of Key Parameters: Having obtained the end-to-end system outage probability O_P in Section IV, an important question arises naturally as to how to properly configure the parameters in order to improve the outage performance of the system. To answer this question, the effects of the key parameters involved, e.g., transmit power P_{LED}, target rate R_t, peak amplitude A, and dc bias B, need to be evaluated.

It is obvious that with a higher P_{LED}, a smaller O_P is achieved, and *vice versa*. However, P_{LED} cannot be increased without a limit, and an unnecessarily high P_{LED} will lead to a low energy utilization efficiency of the system. Similarly, a lower R_t will result in a smaller O_P. However, the selection of R_t depends on many factors, including the application scenarios, modulation schemes, and channel conditions, and is usually predefined. The effects of A and B on O_P, however, are not straightforward, which will be analyzed in the following.

With a summation of $O_P^{(1)}$ and $O_P^{(2)}$ obtained in (15) and (21), respectively, the end-to-end outage probability of the system can be rewritten as

$$O_P = 1 - \int_0^{E_{\max}} \alpha E_R^{\frac{-n-4}{n+3}}e^{\frac{-\beta}{E_R}}dE_R + \int_0^{E_{1,\mathrm{th}}} \alpha E_R^{\frac{-n-4}{n+3}}e^{\frac{-\beta}{E_R}}dE_R. \tag{26}$$

From (26), the partial derivative of O_P with respect to A can be derived as

$$\frac{\partial O_P}{\partial A} = \frac{\partial O_P}{\partial E_{1,\mathrm{th}}}\frac{\partial E_{1,\mathrm{th}}}{\partial A}$$

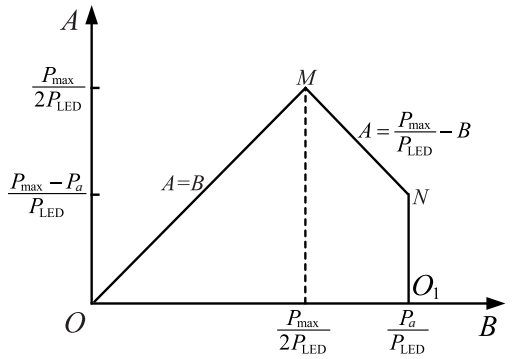

Fig. 2. Feasible region of (B, A) subject to the constraints imposed by both the average and peak powers of the LED source, where $O = (0, 0)$, $M = ([(P_{\max})/(2P_{\text{LED}})], [(P_{\max})/(2P_{\text{LED}})])$, $N = ([(P_a)/(P_{\text{LED}})], [(P_{\max} - P_a)/(P_{\text{LED}})])$, and $O_1 = ([(P_a)/(P_{\text{LED}})], 0)$.

$$= \alpha\left(E_{1,\text{th}}\right)^{\frac{-n-4}{n+3}} e^{\frac{-\beta}{E_{1,\text{th}}}} \frac{-2E_{1,\text{th}}}{A} = \frac{-2\left[\left(r_{1,\text{th}}\right)^2 + l_1^2\right]}{A(n+3)r^2} e^{\frac{-\beta I_0}{fV_t(\rho P_{\text{LED}}B)^2\gamma_{1,\text{th}}}} \le 0 \quad (27)$$

where $\gamma_{1,\text{th}} = [([(n+1)kl_1^{n+1}]^2)/([(r_{1,\text{th}})^2+l_1^2]^{n+3})]$ is obtained from (7) by letting $r_1 = r_{1,\text{th}}$. Similarly, from (26), the partial derivative of O_P with respect to B can be expressed as

$$\begin{aligned}\frac{\partial O_P}{\partial B} &= -\alpha\left(E_{1,\max}\right)^{\frac{-n-4}{n+3}} e^{\frac{-\beta}{E_{1,\max}}} \frac{\partial E_{1,\max}}{\partial B} + \alpha\left(E_{1,\text{th}}\right)^{\frac{-n-4}{n+3}} \times e^{\frac{-\beta}{E_{1,\text{th}}}} \frac{\partial E_{1,\text{th}}}{\partial B} \\ &= \frac{-2}{B(n+3)r^2}\left\{ l_1^2 e^{\frac{-\beta I_0}{fV_t(\rho BP_{\text{LED}})^2\gamma_{1,\max}}} - \left[\left(r_{1,\text{th}}\right)^2 + l_1^2\right] e^{\frac{-\beta I_0}{fV_t(\rho BP_{\text{LED}})^2\gamma_{1,\text{th}}}} \right\} \\ &\le \frac{-2l_1^2}{B(n+3)r^2}\left(e^{\frac{-\beta I_0}{fV_t(\rho BP_{\text{LED}})^2\gamma_{1,\max}}} - e^{\frac{-\beta I_0}{fV_t(\rho BP_{\text{LED}})^2\gamma_{1,\text{th}}}} \right) \\ &\le 0 \end{aligned} \quad (28)$$

where $\gamma_{1,\max} = [([(n+1)kl_1^{n+1}]^2)/(l_1^{2(n+3)})]$ is obtained from (7) by letting $r_1 = 0$. Thus, from (27) and (28), O_P is monotonically decreasing (or nonincreasing) with respect to A and B.

However, in view of the fact that A and B are mutually constrained as given in (3), A or B cannot be increased without a limit and the optimal design of A and B is nontrivial. Next, we formulate the optimization problem of minimizing O_P with respect to A and B.

2) Optimization Problem: Based on the analysis above, the optimization problem of minimizing the end-to-end outage probability can be formulated as

$$\min_{\{A,B\}} O_P, \quad \text{s.t. } B \le \frac{P_a}{P_{\text{LED}}},\ A \le \min\left\{B, \frac{P_{\max}}{P_{\text{LED}}} - B\right\}. \quad (29)$$

To provide insights into this problem, the feasible region of A and B is illustrated in Fig. 2.

Remark 1: From Fig. 2, in the left part of the feasible region under $\overline{OM}$, it is obvious that O_P can be effectively reduced by increasing A and B simultaneously along the line of $A = B$. In other words, O_P reaches the local minimum at the vertex of M. In the right part of the feasible region under $\overline{MN}$, however, it is observed that A and B are mutually constrained by the line of $A = [(P_{\max})/(P_{\text{LED}})] - B$, which results in a performance tradeoff between the first and second hop transmissions. To be specific, with an increase in B, although more energy E_R will be available for improving the performance of the second-hop transmission $R \to D$, the corresponding reduction in A will degrade the performance of the first-hop transmission $S \to R$. Moreover, on the line of $\overline{NO_1}$ where B is constant and A reaches the maximum at the vertex of N, it is obvious that O_P reaches the local minimum at N.

From the above discussions, the information flow and the energy flow need to be dynamically matched for reaching a balance between the performances of the VLC and RF transmissions over the two hops. This requires a joint design of (B, A), as will be analyzed in detail in the following.

B. Joint Design of the Optimal (B^*, A^*)

Since A is an important factor of the channel capacity C_1 as given in (9), for S to successfully decode $x(t)$ in the first hop, i.e., $C_1 \ge R_t$, we have equivalently

$$A \ge A_{\text{th}} = \frac{\left[2\pi e\lambda_1\sigma_1^2\left(r_1^2 + l_1^2\right)^{n+3}\right]^{\frac{1}{2}}}{\rho P_{\text{LED}}(n+1)kl_1^{n+1}}. \quad (30)$$

This means that the source signal $x(t)$ can be successfully decoded by R only if A is above a certain threshold A_{th}. Since R is randomly located within the circular area, we consider two extreme scenarios where R is located at the center and the edge of the circular area, i.e., $r_1 = 0$ and $r_1 = r$, respectively. Then, substituting $r_1 = 0$ and $r_1 = r$ into (30), we obtain

$$A_{\text{th}}^{\text{low}} = \frac{\left[2\pi e\lambda_1\sigma_1^2 l_1^{2(n+3)}\right]^{\frac{1}{2}}}{\rho P_{\text{LED}}(n+1)kl_1^{n+1}} \quad (31)$$

$$A_{\text{th}}^{\text{upp}} = \frac{\left[2\pi e\lambda_1\sigma_1^2\left(r^2 + l_1^2\right)^{n+3}\right]^{\frac{1}{2}}}{\rho P_{\text{LED}}(n+1)kl_1^{n+1}} \quad (32)$$

respectively. Here, $A_{\text{th}}^{\text{low}}$ denotes the threshold of A below which $x(t)$ cannot be decoded by S even when it is located at the center of the circular area, and $A_{\text{th}}^{\text{upp}}$ denotes the threshold of A above which $x(t)$ can be successfully decoded by R even when it is located at the edge of the circular area. Thus, a suitable A needs to be selected in between $A_{\text{th}}^{\text{low}}$ and $A_{\text{th}}^{\text{upp}}$.

Depending on the relationship of A, $A_{\text{th}}^{\text{low}}$, and $A_{\text{th}}^{\text{upp}}$, we have the following cases in which (B^*, A^*) is analyzed.

1) $A_{th}^{low} > [(P_{max})/(2P_{LED})]$: For this case 1), from (31), we have

$$R_t > C_1\left(r_1 = 0, A = \frac{P_{\max}}{2P_{\text{LED}}}\right) = \tau\log_2\left(1 + \frac{\left[\rho P_{\max}(n+1)kl_1^{n+1}\right]^2}{8\pi e\sigma_1^2 l_1^{2(n+3)}}\right) \quad (33)$$

equivalently. This means that with a very high target rate where

$$R_{\rm t} > \tau \log_2\left(1+\frac{\left[\rho P_{\max}(n+1)kl_1^{n+1}\right]^2}{8\pi e\sigma_1^2 l_1^{2(n+3)}}\right)$$

even if A takes the maximum allowed value of $[(P_{\max})/(2P_{\rm LED})]$, $x(t)$ cannot be decoded by S even when it is located at the center of the circular area. Thus, we have the corresponding outage probabilities

$$O_P^{(1)} = 1, \quad O_P = 1 \tag{34}$$

throughout the feasible region of (B, A).

2) $A_{th}^{low} \le [(P_{max})/(2P_{LED})] < A_{th}^{upp}$*:* For this case 2), from (31) and (32), we can equivalently obtain (35), shown at the bottom of the page. This means that with a moderate R_t where

$$\tau \log_2\left(1+\frac{\left[\rho P_{\max}(n+1)kl_1^{n+1}\right]^2}{8\pi e\sigma_1^2 (r^2+l_1^2)^{n+3}}\right) < R_{\rm t} \le \tau \log_2\left(1+\frac{\left[\rho P_{\max}(n+1)kl_1^{n+1}\right]^2}{8\pi e\sigma_1^2 l_1^{2(n+3)}}\right),$$

$x(t)$ can be successfully decoded by S when it is located at the center of the circular area (i.e., $r_1 = 0$), but cannot be decoded by S when it is located at the edge of the circular area (i.e., $r_1 = r$). Thus, we have the corresponding outage probabilities

$$0 < O_P^{(1)} < 1, \quad O_P = O_P^{(1)} + O_P^{(2)}. \tag{36}$$

Thus, a performance tradeoff exists between the two successive hops, which should be jointly considered to minimize O_P.

As shown in Fig. 3, this case can be further divided into two subcases, with the respective intersection points $N_1 = ([(P_{\max})/(P_{\rm LED})] - A_{\rm th}^{\rm low}, A_{\rm th}^{\rm low})$ and $N_2 = ([(P_a)/(P_{\rm LED})], A_{\rm th}^{\rm low})$, as detailed in the following.

a) $[(P_{max} - P_a)/(P_{LED})] < A_{th}^{low} \le [(P_{max})/(2P_{LED})] < A_{th}^{upp}$*:* For this case 2a), as shown in Fig. 3(a), we can equivalently obtain (37), shown at the bottom of the page. Then, it is apparent that the optimal (B^*, A^*) lies on $\overline{MN_1}$. Due to

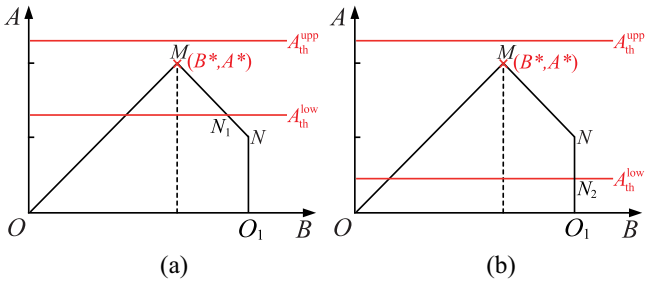

Fig. 3. Illustration of case 2) where $x(t)$ can be successfully decoded by R when it is located at the center of the circular area (i.e., $r_1 = 0$), but cannot be decoded by R when it is located at the edge of the circular area (i.e., $r_1 = r$), for which we have $A_{\rm th}^{\rm low} \le [(P_{\max})/(2P_{\rm LED})] < A_{\rm th}^{\rm upp}$ equivalently. (a) When $[(P_{\max} - P_a)/(P_{\rm LED})] < A_{\rm th}^{\rm low} \le [(P_{\max})/(2P_{\rm LED})] < A_{\rm th}^{\rm upp}$. (b) When $A_{\rm th}^{\rm low} < [(P_{\max} - P_a)/(P_{\rm LED})] < [(P_{\max})/(2P_{\rm LED})] < A_{\rm th}^{\rm upp}$.

the complex form of O_P as given in (23), it is intractable to directly analyze the monotonicity of O_P on $\overrightarrow{MN_1}$. Substituting $A = [(P_{\max})/(P_{\rm LED})] - B$ into (23), O_P can be rewritten as [61]

$$O_P = 1 - \int_0^{r_{1,\rm th}} \frac{2r_1}{r^2} e^{\frac{-\beta}{E_R}} dr_1. \tag{38}$$

Since $0 < O_P^{(1)} < 1$ and $0 < r_{1,\rm th} < r \ \forall \ A \in [A_{\rm th}^{\rm low}, ([P_{\max}]/[2P_{\rm LED}])]$, the derivative of O_P in (38) with respect to variable B can be derived as [61]

$$\frac{dO_P}{dB} = -\frac{2r_{1,\rm th}}{r^2} e^{\frac{-\beta}{E_{1,\rm th}}} \frac{dr_{1,\rm th}}{dB}. \tag{39}$$

Based on (13), we have the derivative of $r_{1,\rm th}$ with respect to B [61]

$$\frac{dr_{1,\rm th}}{dB} = \frac{1}{2r_{1,\rm th}(n+3)} \times \left\{\frac{\left[\rho(P_{\max} - P_{\rm LED}B)(n+1)kl_1^{n+1}\right]^2}{2\pi e\lambda_1\sigma_1^2}\right\}^{\frac{-n-2}{n+3}} \times \frac{-2P_{\rm LED}\left[\rho(P_{\max} - P_{\rm LED}B)(n+1)kl_1^{n+1}\right]}{2\pi e\lambda_1\sigma_1^2}$$

$$\text{Case 2)}: \ C_1\left(r_1 = r, A = \frac{P_{\max}}{2P_{\rm LED}}\right) < R_t \le C_1\left(r_1 = 0, A = \frac{P_{\max}}{2P_{\rm LED}}\right)$$
$$\Rightarrow \tau \log_2\left(1+\frac{\left[\rho P_{\max}(n+1)kl_1^{n+1}\right]^2}{8\pi e\sigma_1^2\left(r^2+l_1^2\right)^{n+3}}\right) < R_t \le \tau \log_2\left(1+\frac{\left[\rho P_{\max}(n+1)kl_1^{n+1}\right]^2}{8\pi e\sigma_1^2 l_1^{2(n+3)}}\right) \tag{35}$$

$$\text{Case2a)}: \ C_1\left(r_1 = 0, A = \frac{P_{\max} - P_a}{P_{\rm LED}}\right) < R_t \le C_1\left(r_1 = 0, A = \frac{P_{\max}}{2P_{\rm LED}}\right)$$
$$\Rightarrow \tau \log_2\left(1+\frac{\left[\rho(P_{\max} - P_a)(n+1)kl_1^{n+1}\right]^2}{2\pi e\sigma_1^2\left(r^2+l_1^2\right)^{n+3}}\right) < R_t \le \tau \log_2\left(1+\frac{\left[\rho P_{\max}(n+1)kl_1^{n+1}\right]^2}{8\pi e\sigma_1^2 l_1^{2(n+3)}}\right) \tag{37}$$

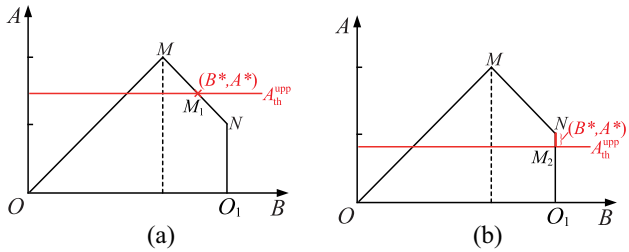

Fig. 4. Illustration of case 3) where $x(t)$ can be successfully decoded by R by selecting a suitable A, for which we have $A_{\text{th}}^{\text{upp}} \le [P_{\max}/(2P_{\text{LED}})]$ equivalently. (a) When $[(P_{\max} - P_a)/P_{\text{LED}}] < A_{\text{th}}^{\text{upp}} \le [P_{\max}/(2P_{\text{LED}})]$. (b) When $A_{\text{th}}^{\text{upp}} \le [(P_{\max} - P_a)/P_{\text{LED}}]$.

$$= \frac{-P_{\text{LED}}\left[\rho(P_{\max} - P_{\text{LED}}B)(n+1)kl_1^{n+1}\right]^{\frac{-n-1}{n+3}}}{r_{1,\text{th}}(n+3)\left(2\pi e\lambda_1\sigma_1^2\right)^{\frac{1}{n+3}}} \le 0. \tag{40}$$

Substituting (40) into (39), we have

$$\frac{dO_P}{dB} = \frac{2e^{\frac{-\beta}{E_{1,\text{th}}}}P_{\text{LED}}\left[\rho(P_{\max}-P_{\text{LED}}B)(n+1)kl_1^{n+1}\right]^{\frac{-n-1}{n+3}}}{r^2(n+3)\left(2\pi e\lambda_1\sigma_1^2\right)^{\frac{1}{n+3}}} \ge 0. \tag{41}$$

From the above analysis, since O_P increases monotonically on $\overrightarrow{MN_1}$, we obtain the optimal $(B^*, A^*) = ([(P_{\max})/(2P_{\text{LED}})], [(P_{\max})/(2P_{\text{LED}})])$, which is located at vertex M.

b) $A_{th}^{low} \le [(P_{max} - P_a)/(P_{LED})] < [(P_{max})/(2P_{LED})] < A_{th}^{upp}$*:* For this case 2b), as shown in Fig. 3(b), we can equivalently obtain (42), shown at the bottom of the page. Following the same line as above, it can be proved that O_P increases monotonically on $\overrightarrow{MN}$. The details are omitted here due to space constraint. Thus, we obtain the optimal $(B^*, A^*) = ([(P_{\max})/(2P_{\text{LED}})], [(P_{\max})/(2P_{\text{LED}})])$, which is located at vertex M.

3) $A_{th}^{upp} \le [(P_{max})/(2P_{LED})]$*:* For this case 3), from (32), we can obtain

$$R_t \le C_1\left(r_1 = r, A = \frac{P_{\max}}{2P_{\text{LED}}}\right) = \tau \log_2\left(1 + \frac{\left[\rho P_{\max}(n+1)kl_1^{n+1}\right]^2}{8\pi e\sigma_1^2\left(r^2+l_1^2\right)^{n+3}}\right) \tag{43}$$

equivalently. This means that with a relatively low target rate where

$$R_{\text{t}} \le \tau \log_2\left(1 + \frac{\left[\rho P_{\max}(n+1)kl_1^{n+1}\right]^2}{8\pi e\sigma_1^2\left(r^2+l_1^2\right)^{n+3}}\right)$$

it is possible to select a suitable A (but not necessarily the maximum allowed $A = [(P_{\max})/(2P_{\text{LED}})]$), which enables $x(t)$ to be successfully decoded by S even when it is located at the edge of the circular area. Thus, we have the corresponding outage probabilities

$$O_P^{(1)} = 0, \quad O_P = O_P^{(2)}. \tag{44}$$

That is, as long as $A \ge A_{\text{th}}^{\text{upp}}$, perfect decoding can be achieved in the first hop, and then, it is beneficial to keep increasing B until its maximum allowed value is reached.

As shown in Fig. 4, this case can be further divided into two subcases, with the respective intersection points $M_1 = ([(P_{\max} - P_a)/(P_{\text{LED}})] - A_{\text{th}}^{\text{upp}}, A_{\text{th}}^{\text{upp}})$ and $M_2 = ([P_a/P_{\text{LED}}], A_{\text{th}}^{\text{upp}})$, as detailed in the following.

a) $[(P_{max} - P_a)/(P_{LED})] < A_{th}^{upp} \le [(P_{max})/(2P_{LED})]$*:* For this case 3a), as shown in Fig. 4(a), we can equivalently obtain (45), shown at the bottom of this page. Next, we analyze the monotonicity of O_P on $\overrightarrow{MM_1}$ and $\overrightarrow{M_1N}$, respectively.

1) On $\overrightarrow{MM_1}$, since $A \ge A_{\text{th}}^{\text{upp}}$, we have $O_P^{(1)} = 0$ and $r_{1,\text{th}} = r$. Then, from (38), we have [61]

$$\begin{aligned}\frac{dO_P}{dB} &= -\frac{d\left(\int_0^r \frac{2r_1}{r^2}e^{\frac{-\beta}{E_R}}dr_1\right)}{dB} \\ &= -\int_0^r \frac{2r_1}{r^2}e^{\frac{-\beta}{E_R}}\frac{\beta}{E_R^2}\frac{dE_R}{dB}dr_1 \\ &= -\int_0^r \frac{2r_1}{r^2}e^{\frac{-\beta}{E_R}}\frac{\beta}{E_R^2} \\ &\quad \times \frac{2BfV_t(\rho P_{\text{LED}})^2\left[(n+1)kl_1^{n+1}\right]^2}{I_0\left(r_1^2+l_1^2\right)^{n+3}}dr_1\end{aligned}$$

$$\text{Case2b)}: C_1\left(r_1 = r, A = \frac{P_{\max}}{2P_{\text{LED}}}\right) < R_t \le C_1\left(r_1 = 0, A = \frac{P_{\max} - P_a}{P_{\text{LED}}}\right) \Rightarrow \tau \log_2\left(1 + \frac{\left[\rho P_{\max}(n+1)kl_1^{n+1}\right]^2}{8\pi e\sigma_1^2\left(r^2+l_1^2\right)^{n+3}}\right) < R_t \le \tau \log_2\left(1 + \frac{\left[\rho(P_{\max}-P_a)(n+1)kl_1^{n+1}\right]^2}{2\pi e\sigma_1^2 l_1^{2(n+3)}}\right) \tag{42}$$

$$\text{Case3a)}: C_1\left(r_1 = r, A = \frac{P_{\max} - P_a}{P_{\text{LED}}}\right) < R_t \le C_1\left(r_1 = r, A = \frac{P_{\max}}{2P_{\text{LED}}}\right) \Rightarrow \tau \log_2\left(1 + \frac{\left[\rho(P_{\max}-P_a)(n+1)kl_1^{n+1}\right]^2}{2\pi e\sigma_1^2\left(r^2+l_1^2\right)^{n+3}}\right) < R_t \le \tau \log_2\left(1 + \frac{\left[\rho P_{\max}(n+1)kl_1^{n+1}\right]^2}{8\pi e\sigma_1^2 l_1^{2(n+3)}}\right) \tag{45}$$

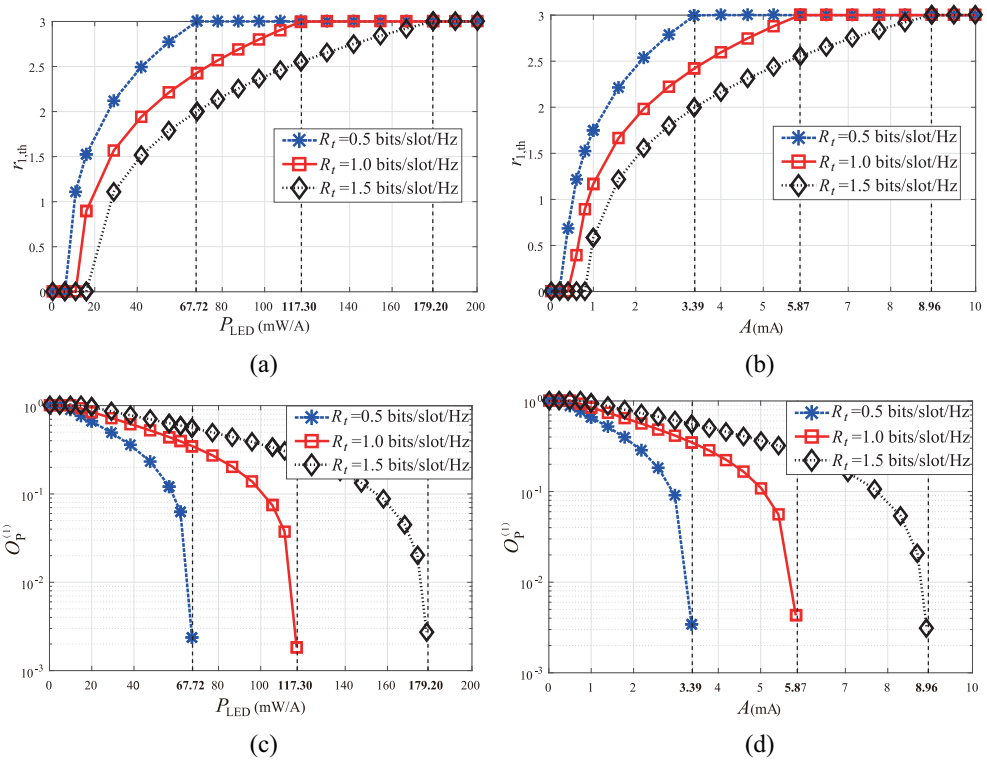

Fig. 5. Illustration of the relay distance threshold $r_{1,\text{th}}$ and the average outage probability $O_P^{(1)}$, where the impacts of the transmit power P_{LED} and the peak amplitude A are evaluated under different values of target rate R_t. (a) $r_{1,\text{th}}$ versus P_{LED}. (b) $r_{1,\text{th}}$ versus A. (c) $O_P^{(1)}$ versus P_{LED}. (d) $O_P^{(1)}$ versus A.

$$= -\int_0^r \frac{4r_1\beta}{r^2 E_R B} e^{\frac{-\beta}{E_R}} dr_1 \leq 0. \quad (46)$$

Thus, O_P decreases monotonically on $\overrightarrow{MM_1}$ and takes the minimum value at M_1.

2) On $\overrightarrow{M_1N}$, since $A < A_{\text{th}}^{\text{upp}}$, we have $0 < O_P^{(1)} \leq 1$ and $0 \leq r_{1,\text{th}} < r$. Following the same line above, it can be proved that $(dO_P/dB) \geq 0$. Thus, O_P increases monotonically on $\overrightarrow{M_1N}$ and takes the minimum value at M_1.

From the above analysis, we obtain the optimal $(B^*, A^*) = ([P_{\max}/P_{\text{LED}}] - A_{\text{th}}^{\text{upp}}, A_{\text{th}}^{\text{upp}})$, which is located at M_1.

b) $A_{th}^{upp} \leq [(P_{max} - P_a)/(P_{LED})]$: For this case 3b), as shown in Fig. 4(b), we have equivalently

$$R_t \leq C_1\left(r_1 = r, A = \frac{P_{\max} - P_a}{P_{\text{LED}}}\right) = \tau \log_2\left(1 + \frac{\left[\rho(P_{\max} - P_a)(n+1)kl_1^{n+1}\right]^2}{2\pi e\sigma_1^2\left(r^2 + l_1^2\right)^{n+3}}\right). \quad (47)$$

From Fig. 4(b), we analyze the monotonicity of O_P on $\overrightarrow{MN}$, $\overrightarrow{NM_2}$, and $\overrightarrow{M_2O_1}$, respectively.

1) On $\overrightarrow{MN}$, since $A \geq A_{\text{th}}^{\text{upp}}$, we have $O_P^{(1)} = 0$ and $r_{1,\text{th}} = r$. Following the same line as in (46), it can be proved that $[(dO_p)/dB] \leq 0$. Thus, O_P decreases monotonically on $\overrightarrow{MN}$ and takes the minimum value at N.

2) On $\overrightarrow{NM_2}$, since $A \geq A_{\text{th}}^{\text{upp}}$, similarly, we have $O_P^{(1)} = 0$ and $r_{1,\text{th}} = r$. Since B is constant on $\overrightarrow{NM_2}$, O_P takes the minimum value along the line of $\overrightarrow{NM_2}$.

3) On $\overrightarrow{M_2O_1}$, it is apparent that O_P takes the minimum value at M_2.

From the above analysis, we obtain the optimal (B^*, A^*) on $\overrightarrow{NM_2}$, where $B^* = [P_a/(P_{\text{LED}})]$ and $A_{\text{th}}^{\text{upp}} \leq A^* \leq [(P_{\max} - P_a)/(P_{\text{LED}})]$.

VI. Simulations

In this section, experiments are conducted to evaluate the performance of the proposed dual-hop hybrid VLC/RF cooperative communication system based on SLIPT. In order to verify the validity of the obtained results, both the analytical results and the Monte Carlo simulation results are presented, which are represented by lines and markers, respectively. For ease of illustration, we use the default values of parameters as listed in Table I, unless otherwise specified.

The relay distance threshold $r_{1,\text{th}}$, as obtained in (13), is demonstrated in Fig. 5(a) and (b) with varying values of P_{LED} and A, respectively. From Fig. 5(a), it is observed that with a higher target rate R_t, it requires a smaller $r_{1,\text{th}}$ for successfully decoding $x(t)$. On the other hand, it is observed that $r_{1,\text{th}}$ increases with P_{LED} and $r_{1,\text{th}} \to r_1 = 3$ m when $P_{\text{LED}} \to 67.72, 117.30, 179.20$ mW/A for $R_t = 0.5, 1.0, 1.5$ bits/slot/Hz, respectively. This means that with a sufficiently high P_{LED}, perfect decoding of $x(t)$ can be achieved at S even when it is located at the edge of the circular area. A similar phenomena can be observed in Fig. 5(b) that given $R_t = 0.5, 1.0, 1.5$ bits/slot/Hz, we have $r_{1,\text{th}} \to 3$ m when $A \to 3.39, 5.87, 8.96$ mA, respectively.

The corresponding outage probability $O_P^{(1)}$ of the first hop transmission, as derived in (15), is also demonstrated in

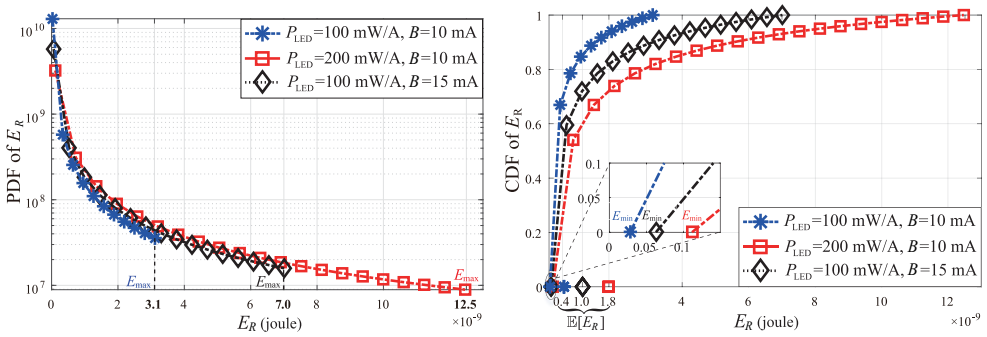

(a) (b)

Fig. 6. Illustration of the PDF and CDF of E_R by taking into account the random locations of R, under different values of $P_{\rm LED}$ and B. (a) PDF of E_R under different values of $P_{\rm LED}$ and B. (b) CDF of E_R under different values of $P_{\rm LED}$ and B.

Fig. 5(c) and (d). As consistent with the results shown in Fig. 5(a) and (b), it is observed that $O_P^{(1)}$ increases with R_t and decreases with $P_{\rm LED}$ and A. Given $R_t = 0.5, 1.0, 1.5$ bits/slot/Hz, respectively, almost perfect decoding of $x(t)$ can be achieved at S, i.e., $O_P^{(1)} \to 0$, when $P_{\rm LED} \to 67.72, 117.30, 179.20$ mW/A or $A \to 3.39, 5.87, 8.96$ mA, respectively.

In view of the random locations of S, the corresponding PDF and the cumulative distribution function (CDF) of the energy harvested by S, i.e., E_R, are demonstrated in Fig. 6(a) and (b), respectively. It is observed that $E_R = E_{\max}$ and $E_R = E_{\min}$ when S is located at the center and at the edge of the circular area, i.e., $r_1 = 0$ and $r_1 = 3$ m, respectively. For a given dc bias B, it is observed that more energy can be harvested by S on average by using a higher LED power $P_{\rm LED}$. Similarly, for a given $P_{\rm LED}$, more energy can be harvested by S on average by using a higher B.

Fig. 7 demonstrates the end-to-end outage probability O_P with varying values of $P_{\rm LED}$, A and τ, respectively. Again, it is observed that the overall performance degrades with an increasing R_t. From Fig. 7(a), it is observed that O_P decreases quickly with $P_{\rm LED}$ in the low-$P_{\rm LED}$ region. However, this improvement becomes slow in the high-$P_{\rm LED}$ region because a higher $P_{\rm LED}$ not only improves $O_P^{(1)}$ in the first hop but also increases E_R, thus significantly improving the end-to-end outage performance. However, when $P_{\rm LED}$ is increased to a certain point above, which $x(t)$ can always be successfully decoded by S, O_P will be bottlenecked by the second hop with limited E_R. Then, it becomes more beneficial to increase the dc bias B, which is able to effectively increase E_R as well as reduce $O_P^{(2)}$. Similar phenomena can be observed in Fig. 7(b), except that no performance improvement can be achieved when A is above a certain point. This is reasonable as when perfect decoding of $x(t)$ is achieved in the first hop, there is no point to keep increasing A that has no benefit to the performance of the second hop. These observations are consistent with the analysis in Section V-B, where A and B need to be jointly designed for reaching a balance between the information flow and the energy flow across the two hops.

To provide more insights, the impact of the time allocation factor τ between the two hops is demonstrated in Fig. 7(c). It is observed that with increasing τ, the overall O_P first decreases, reaches the minimum, and then increases. This is reasonable as in the low-τ regime, the source information can be hardly decoded by S and the first hop transmission $S \to R$ constitutes the performance bottleneck. Then, with an increase in τ, the relay S is able to successfully decode the source information with a higher probability while collecting more energy, thus significantly improving the system performance. However, with an unnecessarily high τ, the second hop transmission $R \to D$ becomes the performance bottleneck due to the limited transmission duration. This implies that in addition to A and B, a suitable τ also needs to be selected for reaching a balance between the performances of the two hops, which will be delegated to our future work. Furthermore, it is observed that with a higher R_t, in general, a higher τ needs to be adopted for efficiently enhancing the end-to-end outage performance. This is reasonable as the relay S has to successfully decode the source information and collect sufficient energy, before the second-hop transmission can be performed.

Fig. 8 demonstrates O_P within the feasible region of (B, A) under different values of R_t, where the optimal (B^*, A^*) is marked that agrees well with the analysis in Section V-B. From Fig. 8(a) where $R_t = 5$ bits/slot/Hz, it corresponds to the case where $[(P_{\max} - P_a)/(P_{\rm LED})] < A_{\rm th}^{\rm low} \le [(P_{\max})/(2P_{\rm LED})] < A_{\rm th}^{\rm upp}$, as illustrated in Fig. 3(a). Then, it is observed that O_P takes the minimum value at $(B^*, A^*) = (20, 20)$, which validates our analysis in Section V-B2. From Fig. 8(b), where $R_t = 3$ bits/slot/Hz, it corresponds to the case where $A_{\rm th}^{\rm low} \le [(P_{\max} - P_a)/(P_{\rm LED})] < [(P_{\max})/(2P_{\rm LED})] < A_{\rm th}^{\rm upp}$, as illustrated in Fig. 3(b). Then, it is observed that O_P takes the minimum value at $(B^*, A^*) = (20, 20)$, which validates our analysis in Section V-B2. From both Fig. 8(a) and (b), it is observed that when $A < A_{\rm th}^{\rm low}$, it is impossible for S to decode the source information even when it is located at the center of the coverage area; thus, the entire system falls into an outage, i.e., $O_P = 1$. Whereas when $A \ge A_{\rm th}^{\rm low}$, it is possible for S to successfully decode the source information, and the overall performance is improved with an increase of A. This implies that in practice, the value of certain parameters needs to be appropriately configured, e.g., $A \ge A_{\rm th}^{\rm low}$, in order to guarantee the proper operation of the system.

From Fig. 8(c), where $R_t = 2$ bits/slot/Hz, it corresponds to the case where $[(P_{\max} - P_a)/(P_{\rm LED})] < A_{\rm th}^{\rm upp} \le$

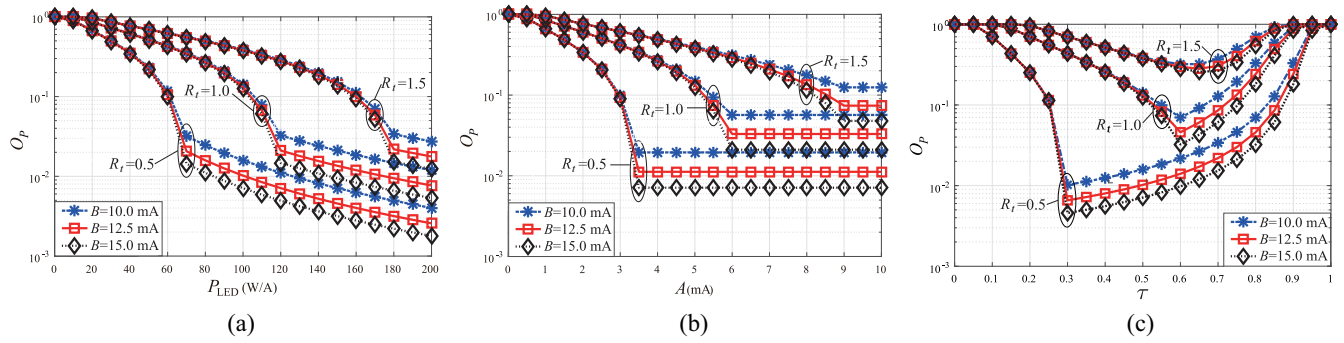

Fig. 7. Illustration of the end-to-end outage probability O_P, where the impacts of the key parameters P_{LED}, R_t, A, B, and τ are evaluated. (a) O_P versus P_{LED} under different values of R_t and B. (b) O_P versus A under different values of R_t and B. (c) O_P versus τ under different values of R_t and B.

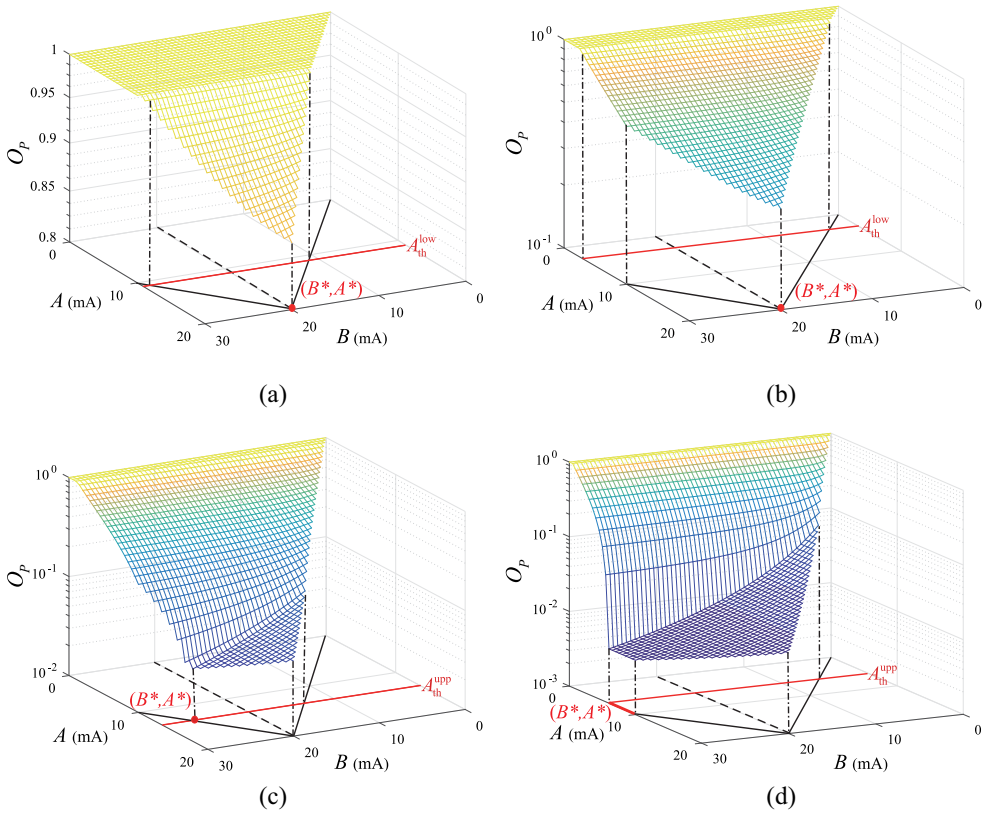

Fig. 8. Illustration of the end-to-end outage probability O_P within the feasible region of (B, A), where the obtained optimal (B^*, A^*) is marked that agrees well with the simulation result. (a) When $R_t = 5$, i.e., $[(P_{\max} - P_a)/(P_{\text{LED}})] < A_{\text{th}}^{\text{low}} \leq [(P_{\max})/(2P_{\text{LED}})] < A_{\text{th}}^{\text{upp}}$. (b) When $R_t = 3$, i.e., $A_{\text{th}}^{\text{low}} \leq [(P_{\max} - P_a)/(P_{\text{LED}})] < [(P_{\max})/(2P_{\text{LED}})] < A_{\text{th}}^{\text{upp}}$. (c) When $R_t = 2$, i.e., $[(P_{\max} - P_a)/(P_{\text{LED}})] < A_{\text{th}}^{\text{upp}} \leq [(P_{\max})/(2P_{\text{LED}})]$. (d) When $R_t = 1$, i.e., $A_{\text{th}}^{\text{upp}} \leq [(P_{\max} - P_a)/(P_{\text{LED}})]$.

$[(P_{\max})/(2P_{\text{LED}})]$, as illustrated Fig. 4(a). Then, it is observed that O_P takes the minimum value at $(B^*, A^*) = (26.5, 13.5)$, which validates our analysis in Section V-B3. From Fig. 8(d), where $R_t = 1$ bit/slot/Hz, it corresponds to the case where $A_{\text{th}}^{\text{upp}} \leq [(P_{\max} - P_a)/(P_{\text{LED}})]$, as illustrated Fig. 4(b). Then, it is observed that O_P takes the minimum value when $B^* = 30$ and $A^* \in [6, 10]$, which validates our analysis in Section V-B3.

For a better illustration of the obtained optimal (B^*, A^*), we consider three baseline schemes within the feasible region, i.e., $(B, A) = (20, 20), (25, 15), (30, 10)$, which correspond to vertex M, middle point between M and N, and vertex N, respectively, as shown in Fig. 2. Then, O_P is demonstrated in Fig. 9(a) with respect to R_t. In the low-R_t region, it is observed that the scheme $(B, A) = (30, 10)$ performs better than the other baseline schemes, which agrees with the analysis in Section V-B3 that the optimal (B^*, A^*) is located on $\overline{NM_2}$. In the mid-R_t region, it is observed that the scheme $(B, A) = (25, 15)$ performs better than the other baseline schemes, which agrees with our analysis in Section V-B3 that the optimal (B^*, A^*) lies in between M and N. In the high-R_t region, it is observed that the scheme $(B, A) = (20, 20)$ performs better than the other baseline schemes, which agrees with our analysis in Section V-B2 that the optimal (B^*, A^*) is located at M. Furthermore, it is worth noting that the proposed

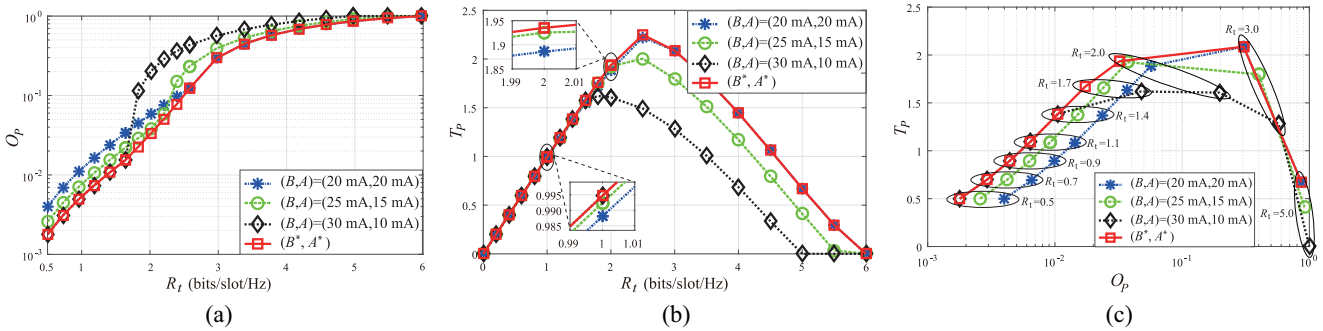

Fig. 9. Illustration of the end-to-end outage probability O_P and the average throughput T_P achieved by the considered system by using the baseline schemes with fixed selection of (B, A) and the obtained optimal (B^*, A^*). (a) O_P versus R_t under four different schemes. (b) T_P versus R_t under four different schemes. (c) T_P versus O_P under four different schemes.

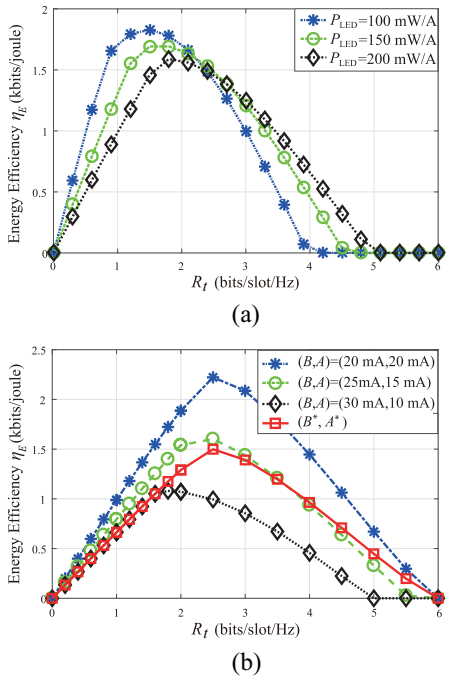

Fig. 10. Illustration of the energy efficiency η_E achieved by the considered system under varying values of the target rate R_t. (a) η_E versus R_t under different values of P_{LED}. (b) η_E versus R_t under four different schemes.

optimal (B^*, A^*) is able to adapt to the varying values of R_t, thus leading to a better performance than the baseline schemes with static selection of (B, A). To be specific, compared to the baseline scheme $(B, A) = (30, 10)$ where $O_P = 0.204$ is achieved at $R_t = 2$ bits/slot/Hz, the corresponding outage probability is reduced by 83.3% by the proposed optimal (B^*, A^*) where $O_P = 0.034$.

The average throughput T_P is also demonstrated in Fig. 9(b). A similar phenomena can be observed that in the low-R_t, mid-R_t, and high-R_t regions, respectively, the scheme of $(B, A) = (30, 10)$, $(25, 15)$, and $(20, 20)$ achieves a higher T_P. Again, the best throughput performance is achieved by the optimal scheme (B^*, A^*) throughout the whole range of R_t. To be specific, compared to the baseline scheme $(B, A) = (30, 10)$ where $T_P = 1.607$ bits/slot/Hz is achieved at $R_t = 2$ bits/slot/Hz, the corresponding throughput is increased by 20.4% by the proposed optimal (B^*, A^*) where $T_P = 1.935$ bits/slot/Hz. Furthermore, it is observed that with increasing R_t, T_P first increases, reaches the maximum, and then decreases. This is reasonable as T_P is limited by the low R_t in the low-R_t region, and limited by the high O_P in the high-R_t region, respectively. This implies that in practice, R_t needs to be properly selected to reach a balance between the outage and throughput of the system.

By combining the results in Fig. 9(a) and (b), T_P is demonstrated versus O_P in Fig. 9(c). With increasing R_t, it is observed that a performance tradeoff exists between T_P and O_P, and they cannot reach the optimum simultaneously. However, with an unnecessarily high R_t, no performance tradeoff exists any more and both T_P and O_P are severely degraded. Again, given an arbitrary R_t, the optimal scheme (B^*, A^*) achieves the best performance.

Furthermore, the system energy efficiency η_E, as derived in (25), is also plotted in Fig. 10. From Fig. 10(a), it is observed that with increasing R_t, the overall η_E first increases, reaches the maximum, and then decreases, which follows the similar trend as that of the average throughput T_P shown in Fig. 9(b). On the other hand, while it is beneficial to adopt a relatively low P_{LED} in the low-R_t region, it is beneficial to adopt a higher P_{LED} with increasing R_t. This indicates that in practice, it would be more energy efficient to adaptively select a suitable transmit power P_{LED} according to the target rate R_t.

The energy efficiency achieved by the proposed (B^*, A^*) is also demonstrated in Fig. 10(b). It is demonstrated that some baseline schemes with fixed (B, A) outperform the proposed (B^*, A^*). This is reasonable in that although the proposed (B^*, A^*) is able to significantly improve the end-to-end outage probability and throughput, it does not necessarily lead to a good performance in terms of the energy efficiency. This also implies that there exists an inherent performance tradeoff between outage and energy efficiency, which cannot reach their optimum simultaneously.

VII. Conclusion

In order to facilitate the application of VLC in IoT subject to the challenges imposed by the constrained coverage and energy, a SLIPT-based dual-hop hybrid VLC/RF cooperative communication system was proposed in this article. To evaluate the performance of the considered system, the

end-to-end outage probability was obtained in a closed-form expression, which is applicable for arbitrary parameter configurations, thereby enabling efficient evaluation of the system performance as well as facilitating the characterization of the impact of key parameters. On this basis, an optimization problem of minimizing the end-to-end outage probability was formulated, subject to practical constraints imposed by both the average and the peak powers of the LED source. This optimization problem was then solved by a joint design of the peak amplitude and the dc bias of the source transmitter, which implies that the information flow and the energy flow need to be dynamically balanced. This was verified by the simulation results, where significant performance gains, in terms of the outage probability and throughput, were achieved by using the obtained optimal solution.

REFERENCES

[1] H. Peng, Q. Li, A. Pandharipande, X. Ge, and J. Zhang, "Performance analysis of a SLIPT-based hybrid VLC/RF system," in *Proc. IEEE/CIC Int. Conf. Commun. China (ICCC)*, Chongqing, China, 2020, pp. 360–365.

[2] F. Javed, M. K. Afzal, M. Sharif, and B.-S. Kim, "Internet of Things (IoT) operating systems support, networking technologies, applications, and challenges: A comparative review," *IEEE Commun. Surveys Tuts.*, vol. 20, no. 3, pp. 2062–2100, 3rd Quart., 2018.

[3] J. Chen, K. Hu, Q. Wang, Y. Sun, Z. Shi, and S. He, "Narrowband Internet of Things: Implementations and applications," *IEEE Internet Things J.*, vol. 4, no. 6, pp. 2309–2314, Dec. 2017.

[4] D. S. Gurjar, H. H. Nguyen, and H. D. Tuan, "Wireless information and power transfer for IoT applications in overlay cognitive radio networks," *IEEE Internet Things J.*, vol. 6, no. 2, pp. 3257–3270, Apr. 2019.

[5] Y. Gao, Z. Qin, Z. Feng, Q. Zhang, O. Holland, and M. Dohler, "Scalable and reliable IoT enabled by dynamic spectrum management for M2M in LTE-A," *IEEE Internet Things J.*, vol. 3, no. 6, pp. 1135–1145, Dec. 2016.

[6] X. Ge, B. Yang, J. Ye, G. Mao, C.-X. Wang, and T. Han, "Spatial spectrum and energy efficiency of random cellular networks," *IEEE Trans. Commun.*, vol. 63, no. 3, pp. 1019–1030, Mar. 2015.

[7] "Cisco vision: 5G—Thriving indoors," Cisco, San Jose, CA, USA, White Paper, 2020. [Online]. Available: https://www.cisco.com/c/dam/en/us/solutions/collateral/service-provider/ultra-services-platform/5g-ran-indoor.pdf

[8] H. Yang, W.-D. Zhong, C. Chen, A. Alphones, and P. Du, "QoS-driven optimized design-based integrated visible light communication and positioning for indoor IoT networks," *IEEE Internet Things J.*, vol. 7, no. 1, pp. 269–283, Jan. 2020.

[9] S. Sepehrvand, L. N. Theagarajan, and S. Hranilovic, "Rate-power tradeoff in simultaneous lightwave information and power transfer systems," *IEEE Commun. Lett.*, vol. 25, no. 4, pp. 1249–1253, Apr. 2021.

[10] J. Gancarz, H. Elgala, and T. D. C. Little, "Impact of lighting requirements on VLC systems," *IEEE Commun. Mag.*, vol. 51, no. 12, pp. 34–41, Dec. 2013.

[11] X. Liu, Y. Wang, F. Zhou, S. Ma, R. Q. Hu, and D. W. K. Ng, "Beamforming design for secure MISO visible light communication networks with SLIPT," *IEEE Trans. Commun.*, vol. 68, no. 12, pp. 7795–7809, Dec. 2020.

[12] A. Tsiatmas, C. P. M. J. Baggen, F. M. J. Willems, J.-P. M. G. Linnartz, and J. W. M. Bergmans, "An illumination perspective on visible light communications," *IEEE Commun. Mag.*, vol. 52, no. 7, pp. 64–71, Jul. 2014.

[13] A. Jovicic, J. Li, and T. Richardson, "Visible light communication: Opportunities, challenges and the path to market," *IEEE Commun. Mag.*, vol. 51, no. 12, pp. 26–32, Dec. 2013.

[14] P. H. Pathak, X. Feng, P. Hu, and P. Mohapatra, "Visible light communication, networking, and sensing: A survey, potential and challenges," *IEEE Commun. Surveys Tuts.*, vol. 17, no. 4, pp. 2047–2077, 4th Quart., 2015.

[15] H. Guo *et al.*, "FPGA implementation of VLC communication technology," in *Proc. 31st Int. Conf. Adv. Inf. Netw. Appl. Workshops (WAINA)*, Taipei, Taiwan, 2017, pp. 586–590.

[16] K. Warmerdam, A. Pandharipande, and D. Caicedo, "Connectivity in IoT indoor lighting systems with visible light communications," in *Proc. IEEE Online Conf. Green Commun. (OnlineGreenComm)*, Piscataway, NJ, USA, 2015, pp. 47–52.

[17] K. Warmerdam, A. Pandharipande, D. Caicedo, and M. Zuniga, "Visible light communications for sensing and lighting control," *IEEE Sensors J.*, vol. 16, no. 17, pp. 6718–6726, Sep. 2016.

[18] A. Khreishah, S. Shao, A. Gharaibeh, M. Ayyash, H. Elgala, and N. Ansari, "A hybrid RF-VLC system for energy efficient wireless access," *IEEE Trans. Green Commun. Netw.*, vol. 2, no. 4, pp. 932–944, Dec. 2018.

[19] T. Rakia, H.-C. Yang, F. Gebali, and M.-S. Alouini, "Optimal design of dual-hop VLC/RF communication system with energy harvesting," *IEEE Commun. Lett.*, vol. 20, no. 10, pp. 1979–1982, Oct. 2016.

[20] C. Zhang, J. Ye, G. Pan, and Z. Ding, "Cooperative hybrid VLC-RF systems with spatially random terminals," *IEEE Trans. Commun.*, vol. 66, no. 12, pp. 6396–6408, Dec. 2018.

[21] G. Pan, H. Lei, Z. Ding, and Q. Ni, "3-D hybrid VLC-RF indoor IoT systems with light energy harvesting," *IEEE Trans. Green Commun. Netw.*, vol. 3, no. 3, pp. 853–865, Sep. 2019.

[22] S. Arnon, *Visible Light Communication*. Cambridge, U.K.: Cambridge Univ. Press, 2015.

[23] G. Nauryzbayev, M. Abdallah, I. S. Ansari, N. Al-Dhahir, and K. Qaraqe, "Outage of cognitive electric vehicle networks over mixed RF/VLC channels with signal-dependent noise and imperfect CSI," *IEEE Trans. Veh. Technol.*, vol. 69, no. 6, pp. 6828–6832, Jun. 2020.

[24] S. H. Chae, C. Jeong, and S. H. Lim. "Simultaneous wireless information and power transfer for Internet of Things sensor networks," *IEEE Internet Things J.*, vol. 5, no. 4, pp. 2829–2843, Aug. 2018.

[25] Q. Li, S. Feng, A. Pandharipande, X. Ge, Q. Ni, and J. Zhan, "Wireless-powered cooperative multi-relay systems with relay selection," *IEEE Access*, vol. 5, pp. 19058–19071, 2017.

[26] R. V. Prasad, S. Devasenapathy, V. S. Rao, and J. Vazifehdan, "Reincarnation in the ambiance: Devices and networks with energy harvesting," *IEEE Commun. Surveys Tuts.*, vol. 16, no. 1, pp. 195–213, 1st Quart., 2014.

[27] M.-L. Ku, W. Li, Y. Chen, and K. J. R. Liu, "Advances in energy harvesting communications: Past, present, and future challenges," *IEEE Commun. Surveys Tuts.*, vol. 18, no. 2, pp. 1384–1412, 2nd Quart., 2016.

[28] D. K. P. Asiedu, H. Lee, and K.-J. Lee, "Simultaneous wireless information and power transfer for decode-and-forward multihop relay systems in energy-constrained IoT networks," *IEEE Internet Things J.*, vol. 6, no. 6, pp. 9413–9426, Dec. 2019.

[29] Q. Li, X. Zhang, A. Pandharipande, X. Ge, and H. Gharavi, "An energy-aware retransmission approach in SWIPT-based cognitive relay systems," *IEEE Trans. Cogn. Commun. Netw.*, vol. 5, no. 3, pp. 580–594, Sep. 2019.

[30] Y. Li, N. Huang, J. Wang, Z. Yang, and W. Xu, "Sum rate maximization for VLC systems with simultaneous wireless information and power transfer," *IEEE Photon. Technol. Lett.*, vol. 29, no. 6, pp. 531–534, Mar. 15, 2017.

[31] G. Pan, J. Ye, and Z. Ding, "Secure hybrid VLC-RF systems with light energy harvesting," *IEEE Trans. Commun.*, vol. 65, no. 10, pp. 4348–4359, Oct. 2017.

[32] P. D. Diamantoulakis, G. K. Karagiannidis, and Z. Ding, "Simultaneous lightwave information and power transfer (SLIPT)," *IEEE Trans. Green Commun. Netw.*, vol. 2, no. 3, pp. 764–773, Sep. 2018.

[33] J. Luo, L. Fan, and H. Li, "Indoor positioning systems based on visible light communication: State of the art," *IEEE Commun. Surveys Tuts.*, vol. 19, no. 4, pp. 2871–2893, 4th Quart., 2017.

[34] Y. Zhuang *et al.*, "A survey of positioning systems using visible LED lights," *IEEE Commun. Surveys Tuts.*, vol. 20, no. 3, pp. 1963–1988, 3rd Quart., 2018.

[35] K. Gligorić, M. Ajmani, D. Vukobratović, and S. Sinanović, "Visible light communications-based indoor positioning via compressed sensing," *IEEE Commun. Lett.*, vol. 22, no. 7, pp. 1410–1413, Jul. 2018.

[36] H. Haas, L. Yin, Y. Wang, and C. Chen, "What is LiFi?" *J. Lightw. Technol.*, vol. 34, no. 6, pp. 1533–1544, Mar. 15, 2016.

[37] P. K. Sharma, Y.-S. Jeong, and J. H. Park, "EH-HL: Effective communication model by integrated EH-WSN and hybrid LiFi/WiFi for IoT," *IEEE Internet Things J.*, vol. 5, no. 3, pp. 1719–1726, Jun. 2018.

[38] Q. Huang, Y. Zhang, Z. Ge, and C. Lu, "Refining Wi-Fi based indoor localization with Li-Fi assisted model calibration in smart buildings," in *Proc. Int. Conf. Comput. Civil Build. Eng. (ICCCBE)*, 2016, pp. 1358–1365.

[39] G. Pan, P. D. Diamantoulakis, Z. Ma, Z. Ding, and G. K. Karagiannidis, "Simultaneous lightwave information and power transfer: Policies, techniques, and future directions," *IEEE Access*, vol. 7, pp. 28250–28257, 2019.
[40] H. G. Sandalidis, A. Vavoulas, T. A. Tsiftsis, and N. Vaiopoulos, "Illumination, data transmission, and energy harvesting: The threefold advantage of VLC," *Appl. Opt.*, vol. 56, no. 12, pp. 3421–3427, Apr. 2017.
[41] J.-Y. Wang, S.-H. Lin, Y. Qiu, N. Huang, and J.-B. Wang, "Tradeoff between secrecy capacity and harvested energy for secure visible light communications with SWIPT," *IEEE Access*, vol. 7, pp. 29543–29552, 2019.
[42] A. M. Abdelhady, O. Amin, B. Shihada, and M.-S. Alouini, "Spectral efficiency and energy harvesting in multi-cell SLIPT systems," *IEEE Trans. Wireless Commun.*, vol. 19, no. 5, pp. 3304–3318, May 2020.
[43] S. Ma, F. Zhang, H. Li, F. Zhou, Y. Wang, and S. Li, "Simultaneous lightwave information and power transfer in visible light communication systems," *IEEE Trans. Wireless Commun.*, vol. 18, no. 12, pp. 5818–5830, Dec. 2019.
[44] T. Rakia, H.-C. Yang, F. Gebali, and M.-S. Alouini, "Dual-hop VLC/RF transmission system with energy harvesting relay under delay constraint," in *Proc. IEEE Globecom Workshops (GC Wkshps)*, Washington, DC, USA, 2016, pp. 1–6.
[45] G. Pan, H. Lei, Z. Ding, and Q. Ni, "On 3-D hybrid VLC-RF systems with light energy harvesting and OMA scheme over RF links," in *Proc. IEEE Global Commun. Conf. (GLOBECOM)*, Singapore, 2017, pp. 1–6.
[46] M. R. Zenaidi, Z. Rezki, M. Abdallah, K. A. Qaraqe, and M.-S. Alouini, "Achievable rate-region of VLC/RF communications with an energy harvesting relay," in *Proc. IEEE Global Commun. Conf. (GLOBECOM)*, Singapore, 2017, pp. 1–7.
[47] Y. Xiao, P. D. Diamantoulakis, Z. Fang, Z. Ma, L. Hao, and G. K. Karagiannidis, "Hybrid lightwave/RF cooperative NOMA networks," *IEEE Trans. Wireless Commun.*, vol. 19, no. 2, pp. 1154–1166, Feb. 2020.
[48] G. Pan, J. Ye, and Z. Ding, "On secure VLC systems with spatially random terminals," *IEEE Commun. Lett.*, vol. 21, no. 3, pp. 492–495, Mar. 2017.
[49] L. Yin, W. O. Popoola, X. Wu, and H. Haas, "Performance evaluation of non-orthogonal multiple access in visible light communication," *IEEE Trans. Commun.*, vol. 64, no. 12, pp. 5162–5175, Dec. 2016.
[50] J.-B. Wang, Q.-S. Hu, J. Wang, M. Chen, and J.-Y. Wang, "Tight bounds on channel capacity for dimmable visible light communications," *IEEE J. Lightw. Technol.*, vol. 31, no. 23, pp. 3771–3779, Dec. 1, 2013.
[51] A. Lapidoth, S. M. Moser, and M. A. Wigger, "On the capacity of free-space optical intensity channels," *IEEE Trans. Inf. Theory*, vol. 55, no. 10, pp. 4449–4461, Oct. 2009.
[52] E. Aparicio-Esteve, Á. Hernández, J. Ureña, and J. M. Villadangos, "Visible light positioning system based on a quadrant photodiode and encoding techniques," *IEEE Trans. Instrum. Meas.*, vol. 69, no. 8, pp. 5589–5603, Aug. 2020.
[53] C. Chen, D. Basnayaka, and H. Haas, "Non-line-of-sight channel impulse response characterisation in visible light communications," in *Proc. IEEE Int. Conf. Commun. (ICC)*, Kuala Lumpur, Malaysia, 2016, pp. 1–6.
[54] W. Gu, M. Aminikashani, P. Deng, and M. Kavehrad, "Impact of multipath reflections on the performance of indoor visible light positioning systems," *IEEE J. Lightw. Technol.*, vol. 34, no. 10, pp. 2578–2587, May 15, 2016.
[55] O. Kallenberg, *Foundations of Modern Probability*, 2nd ed. New York, NY, USA: Springer, 2002.
[56] I. S. Gradshteyn, I. M. Ryzhik, D. Zwillinger, and V. Moll, *Table of Integrals, Series, and Products*, 6th ed. New York, NY, USA: Academic, 2000.
[57] Q. Li, X. Zhang, A. Pandharipande, and J. Zhang, "Cooperative spectrum sharing on SWIPT-based DF relay: An energy-aware retransmission approach," *IEEE Access*, vol. 7, pp. 120802–120816, 2019.
[58] S. Park and D. Hong, "Achievable throughput of energy harvesting cognitive radio networks," *IEEE Trans. Wireless Commun.*, vol. 13, no. 2, pp. 1010–1022, Feb. 2014.
[59] Y. Hei, Y. Kou, G. Shi, W. Li, and H. Gu, "Energy-spectral efficiency tradeoff in DCO-OFDM visible light communication system," *IEEE Trans. Veh. Technol.*, vol. 68, no. 10, pp. 9872–9882, Oct. 2019.
[60] M. Kashef, M. Ismail, M. Abdallah, K. A. Qaraqe, and E. Serpedin "Energy efficient resource allocation for mixed RF/VLC heterogeneous wireless networks," *IEEE J. Sel. Areas Commun.*, vol. 34, no. 4, pp. 883–893, Apr. 2016.
[61] G. B. Thomas, M. D. Weir, F. R. Giordano, and J. Hass, *Thomas' Calculus*, 11th ed. New York, NY, USA: Addison-Wesley, 2005.

Huijie Peng received the B.Eng. degree from the North University of China, Taiyuan, China, in 2017. He is currently pursuing the master's degree with the Huazhong University of Science and Technology, Wuhan, China.

His current research interests include visible light communications, energy harvesting, wireless power transfer, and cooperative communications.

Qiang Li (Member, IEEE) received the B.Eng. degree in communication engineering from the University of Electronic Science and Technology of China, Chengdu, China, in 2007, and the Ph.D. degree in electrical and electronic engineering from Nanyang Technological University, Singapore, in 2011.

From 2011 to 2013, he was a Research Fellow with Nanyang Technological University. Since 2013, he has been an Associate Professor with the Huazhong University of Science and Technology, Wuhan, China, where he has been a Full Professor since 2020. He was a Visiting Scholar with the University of Sheffield, Sheffield, U.K., from March 2015 to June 2015. His current research interests include future broadband wireless networks, cooperative communications, simultaneous wireless/lightwave information and power transfer, fog computing, and edge caching.

Ashish Pandharipande (Senior Member, IEEE) received the M.S. degrees in electrical and computer engineering and mathematics and the Ph.D. degree in electrical and computer engineering from the University of Iowa, Iowa City, IA, USA, in 2000, 2001, and 2002, respectively.

Then, he has been a Postdoctoral Researcher with the University of Florida, Gainesville, FL, USA, a Senior Researcher with the Samsung Advanced Institute of Technology, Suwon, South Korea, and a Senior Scientist with Philips Research, Amsterdam, The Netherlands. He has held visiting positions with AT&T Laboratories, Middletown Township, NJ, USA, and the Department of Electrical Communication Engineering, Indian Institute of Science, Bangalore, India. He is currently a Lead Research and Development Engineer with Signify (new company name of Philips Lighting), Eindhoven, The Netherlands. His research interests are in sensing, cognitive wireless systems, data analytics, machine learning, and system applications.

Dr. Pandharipande is currently a Topical Editor (Sensor Data Processing Area) for IEEE SENSORS JOURNAL, a Senior Editor for IEEE SIGNAL PROCESSING LETTERS, and an Associate Editor for IEEE JOURNAL OF BIOMEDICAL AND HEALTH INFORMATICS and *Lighting Research & Technology Journal*.

Xiaohu Ge (Senior Member, IEEE) received the Ph.D. degree in communication and information engineering from the Huazhong University of Science and Technology (HUST), Wuhan, China, in 2003.

He is currently a Full Professor with the School of Electronic Information and Communications, HUST. He is an Adjunct Professor with the Faculty of Engineering and Information Technology, University of Technology Sydney, Ultimo, NSW, Australia. He has been worked with HUST since November 2005. Prior to that, he worked as a Researcher with Ajou University, Suwon, South Korea, and Politecnico Di Torino, Turin, Italy, from January 2004 to October 2005. He was a Visiting Researcher with Heriot-Watt University, Edinburgh, U.K., from June 2010 to August 2010. He has published about 190 papers in refereed journals and conference proceedings and has been granted about 15 patents in China. His research interests are in the area of mobile communications, traffic modeling in wireless networks, green communications, and interference modeling in wireless communications.

Prof. Ge received the Best Paper Awards from IEEE Globecom 2010. He served as the General Chair for the 2015 IEEE International Conference on Green Computing and Communications. He serves as an Associate Editor for the IEEE WIRELESS COMMUNICATIONS and IEEE TRANSACTIONS ON GREEN COMMUNICATIONS AND NETWORKING.

Jiliang Zhang (Senior Member, IEEE) received the B.E., M.E., and Ph.D. degrees from Harbin Institute of Technology, Harbin, China, in 2007, 2009, and 2014, respectively.

He was a Postdoctoral Fellow with Shenzhen Graduate School, Harbin Institute of Technology from 2014 to 2016, an Associate Professor with the School of Information Science and Engineering, Lanzhou University, Lanzhou, China, from 2017 to 2019, and a Researcher with the Department of Electrical Engineering, Chalmers University of Technology, Gothenburg, Sweden, from 2017 to 2018. He is currently a Marie Curie Research Fellow with the Department of Electronic and Electrical Engineering, The University of Sheffield, Sheffield, U.K. His current research interests include, but are not limited to wireless channel modeling, modulation system, relay system, vehicular communications, ultradense small cell networks, and smart environment modeling.

Dr. Zhang serves as an Academic Editor for the *Wireless Communications and Mobile Computing* and a Topic Editor for *Electronics*.